**King's College London**
7CCMCS01 Individual Research Project

# Arctic region in the weighted random dimer covering

Submission Date: 9th September, 2021

# Abstract

Here we study the effect on the Arctic region of a randomly weighted Aztec diamond lattice first modelling the ground state of the lattice - such that it is the dimer covering with minimal cost, by utilising the Belief Propagation (BP) algorithm . We saw that a randomly weighted Aztec diamond does indeed to have a deterministic Arctic region occurring at the cardinal boundaries of the lattice, such that the edges outside of a limit shape, known as the Arctic circle, would either always be occupied or never occupied - thus having zero variance. Next, excitations could be induced on the ground state dimer covering either within the Arctic region or the Arctic circle, to ascertain the effect of the Arctic region. The excitations caused self-avoiding cycles of lengths dependent on the location of the excitation and along with the size of the lattice. Excitations caused in the Arctic circle showed no likely sign of altering the Arctic region and was thus equivalent to the ground state minus some minor fluctuations in the edge variance. On the other hand, excitations induced in the Arctic region did indeed experience an increase in edges with zero variance, thus increasing the size of the Arctic region.

# Contents

CHAPTER 1

# Introduction

Consider a square lattice of any size with random cost assigned to each edge and imagine a *perfect matching* such that the lattice forms a collection of bijective edges. Each node may only be attached to a single edge while retaining that the sum of all these edges is the minimal collective weight possible - this is a classical combinatorial optimisation process known as the matching problem (MP). Each possible configuration is a dimer covering, but there can only be one minimal cost, and one maximal cost. Though this may seem simple to begin with, an increase in the size escalates the complexity of the problem. Though this model perhaps seems generic, dimer coverings also appear in models and theories in statistical physics [**6**]. Therefore dimer coverings have been widely studied, and for good reason.

There are many approaches and algorithms used to solve the MP, and someone could viably use brute force to find an optimal solution in arbitrarily small graphs; however, when a graph increases in size, such methods become tedious. Here, the Belief Propagation (BP) algorithm will be applied behind the scenes to efficiently find the optimal solution to a MP, and it will very much deserve credit for its application. BP is a message-passing technique used to provide marginal probabilities on a factor graph efficiently - such that each node passes messages iteratively through the graph until the algorithm settles on an optimal solution. BP has been proven to provide correct results and converge with a limited amount of cases; however, it has been shown to efficiently converge to the bipartite Assignment Problem (AP) [**2**][**3**].

Here, the dimer coverings on a randomly weighted Aztec diamond will be approached. The Aztec diamond is not just an interesting shape as opposed to the square lattice, but as its size approaches a higher order, a deterministic limit shape forms within the central region - the *Arctic circle*. At least, this is the case on a random dimer covered Aztec diamond with one-periodic weights, such that vertical edges are weighted 1 and horizontal edges are weighted $a$. Limit shapes have also been observed in other forms of weighted Aztec diamonds, such as two-periodic weighting, and the double Aztec diamond. There remains a gap in the literature on a randomly weighted Aztec diamond, and the effect on the Arctic circle.

Consider a more complicated dimer model by defining the lattice as a substrate, and the nodes as diatomic molecules. The random edge weights may be considered to be their space-dependent binding energy. The importance is to understand how the boundaries of the lattice effects the deposition of the molecules. Therefore, approaching the of diatomic molecules as a randomly weighted Aztec diamond results in a statistical analysis of the behaviour of the system which may be fit and applied to a more realistic model.

In the 1960s, Kasteleyn, and Temperley and Fisher accidentally explored the asymptotic expressions of the number of dimer coverings on an infinite lattice simultaneously [**6**]. Chapter 2 explores dimer coverings - starting from Kasteleyn's approach for a $n \times m$ board, to the structure of the Aztec diamond and to the formation of the Arctic circle.

Chapter 3 will then approach the random AP - which is a commonly applied combinatorial optimisation process for finding the Maximum Weight Matching in a bipartite graph.

Then, it will be shown how BP can be applied to a specific optimisation process, and how the *replica symmetric cavity method* can be approached for utilisation in programming BP.

BP will be used to compute the optimal covering, known as the ground state, of the Aztec diamond. The effect of the random weighted Aztec diamond can be explored through its variance - which will determine the nature of an Arctic region in this model. Excitations are forced on the ground state in different parts of the lattice by removing an edge that occurs in the ground state of the dimer covering. This too will be explored to see how these excitations effect the Arctic region.

CHAPTER 2

# Domino Tilings and Dimer Coverings

## 1. What is a dimer covering?

Given a graph $\mathcal{G}$, a *dimer covering* of $\mathcal{G}$ is a subset of edges which covers every vertex exactly once. In other words, a dimer covering is a perfect matching $M$, subset of the edge set of $\mathcal{G}$, such that each vertex in $\mathcal{G}$ is the endpoint of one edge only in $M$ [**15**]. Such a simple problem has not only been studied in the realm of combinatoric and graph theory, but also physics. The dimer covering problem is a special type of *tiling* problem, performed using a tiling unit as a dimer, or domino - i.e., a unit of two vertices and the edge joining them. Tiling problems have been intensely investigated, and in particular the case of planar graphs, i.e., graphs which can be embedded in the plane [**14**]. As an example, consider Figure 1, an $8 \times 8$ chessboard - it can be modelled as a (bipartite) planar graph such that each black (white) square is associated to a black (white) node of a graph, and edges connect nodes corresponding to adjacent squares. Therefore, any edges connecting two adjacent squares would have one black and one white node. This tiling problem consists in covering the chessboard using $2 \times 1$ and $1 \times 2$ dominoes, where they could not overlap, or equivalently to search for a perfect matching in the corresponding graph:

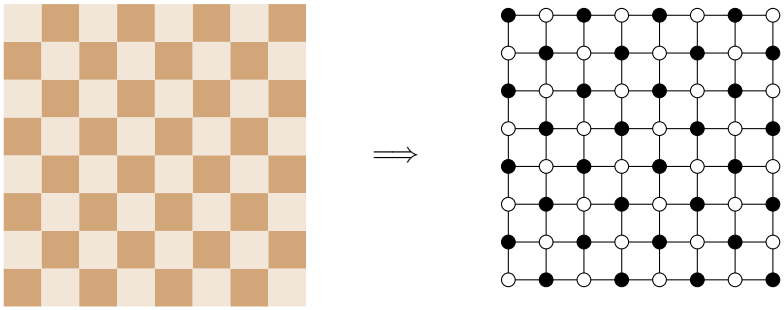

FIGURE 1. 8 by 8 chessboard (left) to a 8 by 8 graph representation of the chessboard (right).

In general, the dominoes become equivalent to dimers, and the grid becomes a lattice; hence, by taking $\mathcal{R}$ as a region bounded by a simple closed polygonal curve in $\mathbb{Z}^2$, a domino tiling of $\mathcal{R}$ correlates to a perfect matching on $\mathcal{G}$, the dual graph of $\mathcal{R}$, such that $\mathcal{G}$ has a vertex for each lattice square in $\mathcal{R}$, with two vertices adjacent if and only if the corresponding lattice squares share an edge [**13**] - this is stating that an edge may only exist if nodes are a single unit apart.

Tilings were originally studied in statistical mechanics as minimal models for diatomic molecules' deposition on a lattice [**15**]. The dominoes are seen to be equivalent to dimers, which are two molecules connected by a bond, and the grid is therefore equivalent to the

deposition lattice. Therefore, it is straight forward to formulate that the arrangement of dominoes on a lattice are convenient because the thermodynamic properties can be formulated from the amount of arrangements where there is a *zero* energy of mixing [**5**].

### 1.1. Counting dimer coverings.

The first question that might arise about dimer coverings on a graph is *how many coverings are possible*. To compute the number of dimer coverings on any bipartite planar graph, an intriguing method called the KTF (Kasteleyn-Temperley-Fisher) method was introduced [**14**]. It is important to note that this method can also be generalised to non-bipartite planar graphs.

1.1.1. *The Boltzmann Measure.*

Considering a finite bipartite planar graph $\mathcal{G} = (B \cup W, \mathcal{E})$, with black nodes set $B = \{\beta_1, ..., \beta_n\}$ and white nodes set $W = \{\alpha_1, ..., \alpha_n\}$, and corresponding edge set $\mathcal{E}$, such that each edge joins nodes of different color only. Giving weights $w$ on the edges as positive real numbers, such that $w : \mathcal{E} \to \mathbb{R}^+$, and with $\mathbb{P} = \mathbb{P}(\mathcal{G}, w)$ a probability measure is defined on the dimer coverings for each dimer covering $M$ of $\mathcal{G}$

$$\mathbb{P}(M) = \frac{1}{Z} \prod_{e \in M} w(e), \tag{1}$$

and where the *partition function* $Z$ is given by:

$$Z = \sum_{M} \prod_{e \in M} w(e). \tag{2}$$

1.1.2. *Kasteleyn's formula.*

Starting with equation 1, Kasteleyn was able to determine the number of possible tilings of any $m \times n$ bipartite planar square lattice. He showed that this number is equal to $\sqrt{|\det K|}$, where $K$ is the weighted adjacency matrix of the graph $G$, called *Kasteleyn matrix* [**12**] [**13**]. The weight of the edges had to be assigned in such a way that, given a black vertex $B$ and a white vertex $W$ [**11**]

$$K(\alpha_i, \beta_j) = \begin{cases} 1 & \text{if } e \text{ is horizontal} \\ i & \text{if } e \text{ is vertical} \\ 0 & \text{otherwise (no edge)} \end{cases}, \tag{3}$$

where $\sqrt{-1} = i$. For the $n \times m$ board, Kasteleyn proved that

$$\sqrt{|\det K|} = \prod_{j=1}^{[\frac{m}{2}]} \prod_{k=1}^{[\frac{n}{2}]} \left( 4\cos^2 \frac{j\pi}{m+1} + 4\cos^2 \frac{k\pi}{n+1} \right). \tag{4}$$

The full derivation of Kasteleyn's formulation can be found in the following references [**12**] [**21**]. As an example, if the number of possible tilings in an $8 \times 8$ chessboard where $n = 8$ and $m = 8$ would be 12,988,816. It is fascinating to break down Kasteleyn's formula and see that it is actually a multiplication of mostly irrational numbers, where the result for the number of tilings is always an integer [**1**].

Furthermore, Kenyon's formula [**11**] [**14**] was used as an extension of the Kastelyn matrix to show the probability of finding a specific dimer configuration, which was given by introducing the inverse Kasteleyn matrix $K^{-1}(\beta_j, \alpha_i)$, showing that the dimers are in fact a determinantal point process.

This particular dimer covering problem is therefore a two-dimensional model that is exactly solvable. Its partition function and correlation functions can be written as the function of determinants at finite volume.

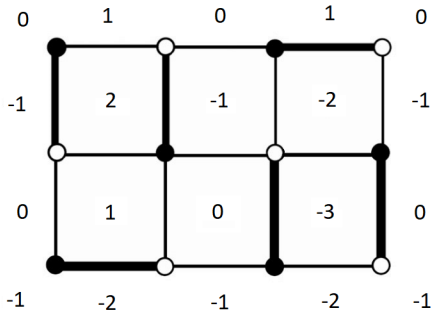


FIGURE 2. Example of the height function on a rectangular lattice.

Kasteleyn's approach can be extended to any finite subset of $\mathbb{Z}^2$ to compute the number of domino tilings. However, this is not stating that any subset of $\mathbb{Z}^2$ can be tiled. A classical example is the mutilated chessboard [**1**] [**19**]. If two diagonally opposite corners of a $n \times n$ chessboard were removed, would a tiling exist? Simply, no - and the reasoning is shown with simple logic. Dealing with a bipartite board, removing two diagonally opposite corners of the board results in an unequal amount of black and white squares. Either two black, or two white squares have been removed, meaning, after any attempt to tile the domain there would be two squares left of the opposite colour. This can also be seen by attempting to find the number of tilings via the determinant. If $K$ is a non-square matrix, then the $\det K = 0$, and there cannot be any dimer covering.

### 1.2. Height Function and Gibbs Measure.

The dimer covering problem is the study of natural measures, or Gibbs Measure, on the set of dimer coverings of a graph, often categorised as a planar graph, for example a subset of $\mathbb{Z}^2$ [**15**], such that, a probability measure on a set of dimer coverings of an infinite size limit is a Gibbs measure - a weak limit of a Boltzmann measure; therefore, for a finite subset of a graph, the probability of a specific set occurring on a finite set will converge. The simplest assumption, in this sense, is to assign *the same weight to all possible dimer coverings of the given graph*, i.e., assume a uniform Gibbs measure over all dimer coverings. Though this model might not be considered entirely realistic for modelling physical processes, it interestingly may allow for an analytical treatment, and may exhibit non-trivial properties [**7**].

A popular approach adopted to study dimer coverings on subsets of $\mathbb{Z}^2$ is to introduce a *height function* [**14**], i.e., a surface defined on the plaquettes of the lattice that is unique for a given dimer covering. The height function is constructed in such a way that crossing an edge occupied by a domino, the height increases by one if the node to the left is white, and decreases by one if the node to the left is black. Using the height function as a third coordinate, a certain class of the random surface model of the domino coverings is obtained in terms of the statistical properties of the height functions induced by the underlying Gibbs measure [**14**]. In particular, by means of the height function, it emerged that there are three types of phases identifiable which depend on the fluctuation properties on the surface. These are classified as *frozen*, *liquid*, and *gaseous* phases. By utilising the height function, an origin point is taken and the height is set to zero. Then the three phases are defined as follows:

**Frozen phase:** the fluctuations of the height functions are deterministic, such that the variance is zero - therefore, these fluctuations are finite regardless of how far from the origin.

**Liquid phase:** the fluctuations of the height function have a variance increasing with increasing distance from the origin.

**Gaseous phase:** the fluctuations of the height function have a bounded variance independently from the origin.

Domino tilings often experience two out of the three phases in the limit shape, which are the frozen phase and the liquid phase [**14**]. Though under specific conditions, a domino tiling may exhibit a gaseous phase, such is seen in the two-periodic weighting of the Aztec diamond [**4**].

### 1.3. The Aztec Diamond.

An Aztec diamond, $A_n$, is defined as the lattice squares contained in $\{(x, y) : |x|+|y| \leq n+1\}$, where $n$ is the order of the Aztec diamond. Examples of various sizes of the Aztec diamond are given in Figure 3.

Consider the Aztec Diamond given in Figure 3 (C) for $n = 8$. The number of nodes in an Aztec diamond graph, it is obtained by stacking successive centred rows of length $2, 4, ..., 2n-2, 2n, 2n, 2n-2, ..., 4, 2$ [**22**].

Therefore, for an Aztec diamond of order $n$, the number of nodes (or unit squares) are given by:

$$2\sum_{k=1}^{n} 2n = 2n(n+1), \tag{5}$$

where $\sum_{k=1}^{n} 2n$ is equal to $n(n+1)$. As an extension, the number of all possible tilings for $A_n$ is given by $2^{n(n+1)/2}$ [**23**]. Therefore, in the case of Figure 3 (C), the graph has exactly 144 nodes, and 262,144 possible coverings, in which one of the possible coverings is shown in Figure 4.

A concurrent study by Temperley and Fisher arrived at the same result, though with a differing methodology, and as a consequence of their individual results, showed that the logarithm of the number of tilings on a $m \times n$ board, divided by the number of dominoes, converges to $2G/\pi \approx 0.58$, and subsequently, in the case of the Aztec diamond that the logarithm of the number of tilings, divided by the number of dominoes, converges to $\log(2)/2 \approx 0.35$. Therefore, by comparing an $m \times n$ board, where $n = m = 68$, and an Aztec diamond of order 64, the number of tilings in the former is greater even though the region of the square board has a slightly smaller area than an Aztec diamond of order 64 [**8**].

1.3.1. *There are four types of dominoes.*

Perhaps not immediately evident in Figure 4, but there are four types of dominoes that occur depending on the orientation of the domino and the location of black and white nodes. Due to the shape of the Aztec diamond, there is a high probability, increased with the order $n$, that there occurs a cluster of specific domino types at each corner, which is called the *Arctic region* [**10**]. The four types are defined as:

(1) West: A domino with vertical orientation where the top node is black and the bottom node is white,
(2) East: a domino with vertical orientation where the top node is white and the bottom node is black,
(3) North: a domino with horizontal orientation where the left node is black and the right node is white,
(4) South: a domino with horizontal orientation where the left node is white and the right node is black.

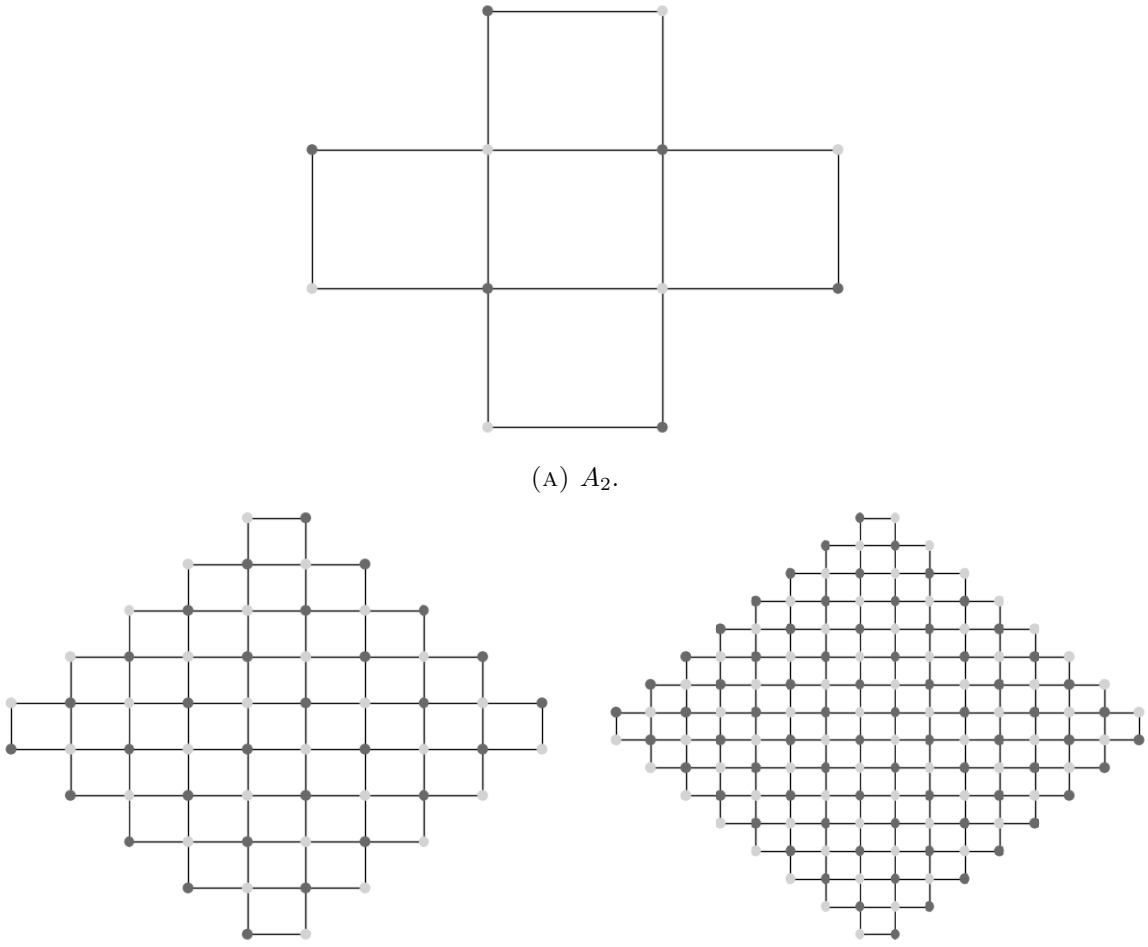

(A) $A_2$.

(B) $A_5$.

(C) $A_8$.

FIGURE 3. A small sample of Aztec diamond sizes $A_n$ for various orders $n$.

Taking the same Aztec diamond dimer covering in Figure 4 and the allocated colours depending on the domino type shown in Figure 5, results in Figure 6.

1.3.2. *The Arctic circle phenomena.*
When $n$ of an Aztec diamond increases, the chance of frozen regions occur with asymptotically high probability; such that, the tilings found at the North, East, South, and West corners become very regular with their respective domino type, as they are out of phase with one another. These regions are called polar regions, i.e., polar North is the frozen region at the north corner of the Aztec diamond. As the distance from the polar regions increase, so do the domino types - the fluctuations of the domino types become somewhat chaotic; hence, entering the temperate region, a liquid phase. This gives the formation of the limit shape known as the *Arctic Circle*. The Arctic circle has in fact been well defined, and occurs in most randomly generated Aztec diamonds [**10**].

Comparing Figure 6 to Figure 7, the existence of a limit shape becomes obvious in higher orders. The Arctic circle centred in the middle of the Aztec Diamond is surrounded by the four polar regions, all with uniformly layered tiles, the *Arctic region*. If $n$ were to

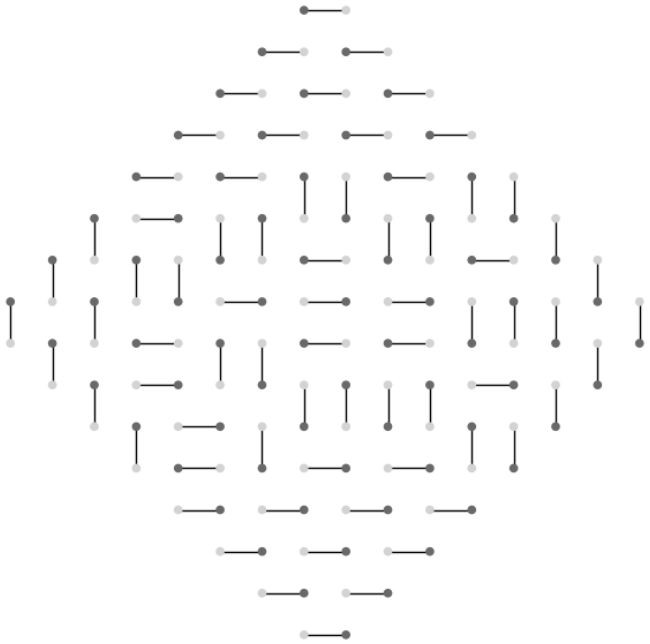

FIGURE 4. Dimer covering of an Aztec diamond of order 8.

(A) North. (B) East. (C) South. (D) West.

FIGURE 5. Colour coordination with respect to the four types of dominoes. Colours are interchangeable as long as they are consistent.

approach infinity, the Arctic circle would become increasingly circular, and the radius of the Arctic circle is known to become arbitrarily close to a perfect circle with $n\sqrt{2}$ [**10**]. In other words, as the order $n \to \infty$ the probability that the occupied edges in a matching developing Arctic regions and a temperate central region increases which converges to the Arctic circle radius of $n\sqrt{2}$.

Using the definitions of the types of dominoes played an important part in proving that an Aztec diamond of order $n$ has exactly $2^{T_n}$ possible tilings [**10**], where $T_n$ is a triangular number defined to be $T_n \equiv \sum_{k=1}^{n} k = \frac{1}{2}n(n+1)$. Furthermore, an algorithm called *shuffling* was used to uniformly generate random domino tilings of the Aztec diamond [**10**].

Shuffling is a stochastic process in which domino tilings of the Aztec diamond of order $n-1$ are turned into various tilings of the Aztec diamond of order $n$. Consider tiling an Aztec diamond of order $n-1$, whereas each domino has been assigned an orientation, as seen previously with the four types of dominoes in Figure 5. If two dominoes share their side of length 2, their assigned direction must be opposite. For example, with an Aztec diamond $n = 1$ one domino must face north or east, while the other faces either south or

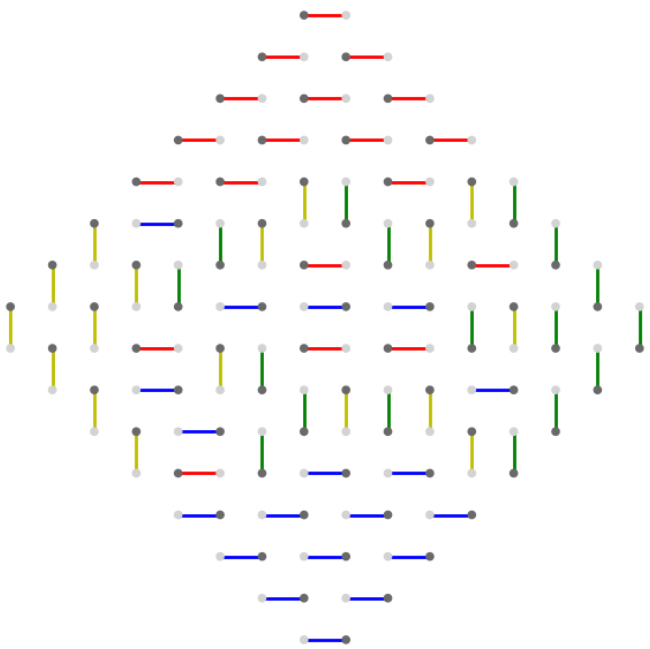

FIGURE 6. The same dimer covering for $n = 8$ in Figure 4 following the domino types.

west. Therefore a directional arrow can be assigned in the centre of the domino with its corresponding direction 8. The dominoes are then defined to be either *good blocks* or *bad block*, where the former is when the arrows are facing away from each other, and the latter is when the arrows are pointing towards each other.

The three steps in shuffling are identified to establish a random tiling of the Aztec diamond. These are known as destruction, sliding, and creation. Destruction occurs when dealing with bad blocks. When the arrows are facing one another as in Figure 8 (A), the two-by-two block is removed from the board, and for sliding, all the good blocks are moved by one unit in the direction of the corresponding arrow. This would then begin to fill an Aztec diamond of order $n$ - however, there remain multiple two-by-two empty blocks. These first two steps ensure that no overlapping dominoes can occur. Therefore, the creation step is a random process that places two dominoes, in the form of a good block, of any orientation to fill in the gaps as seen in Figure 8 (B). The orientation is essentially being determined by a coin flip, and therefore there is a 50% chance that the block consists of a north and south leaning block, or an east and west leaning block. This would result in a complete tiling of $A_n$, an example of the shuffling process is seen in Figure 9. Since all the arrows in the tiling are properly aligned, then the Aztec diamond can be continuously expanded. Shuffling can also be established in reverse, where all good blocks are removed, and the dominoes left slide in the opposite direction.

The iterated shuffling yields a uniform distribution on the set of tilings, where $T$ is the domino tiling of order $n-1$ that has $k(T)$ bad blocks and so $k(T)+n$ good blocks will need to be added in the creation step for the Aztec diamond to have a net increase in area of $2n(n+1) - 2(n-1)n = 4n$. Hence, $T$ retains the possibility of giving any of the $2^{k(T)+n}$ tilings $T'$ of the diamond of order $n$, and each has an equal probability of $2^{-(k(T)+n)}$ [**10**].

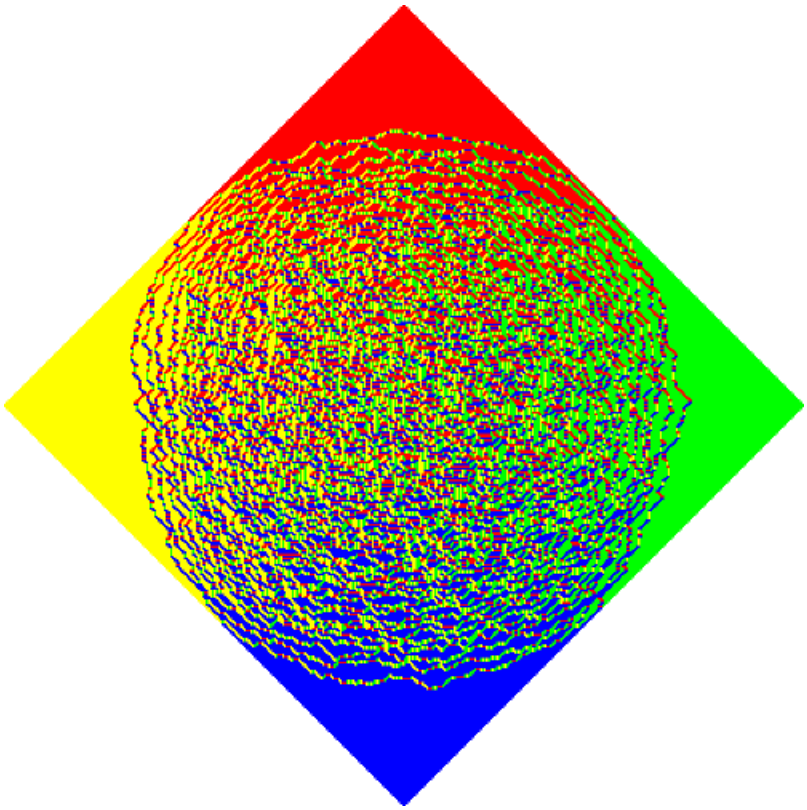

FIGURE 7. A dimer covering of a one-periodic weighted Aztec diamond of order 200. Notably the increase of size results in a smoother looking Arctic circle [**24**].

.

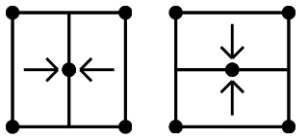

(A) Bad blocks removed during the destruction stage.

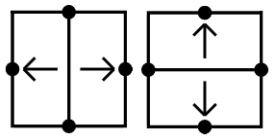

(B) Good blocks formed during the creation stage.

FIGURE 8. Domino blocks that occur during shuffling algorithm. If the arrows are pointing towards each other the block is destroyed (A). Gaps in the Aztec diamond are replaced with dominoes (B) in the creation stage.

Paying attention to the boundaries of the Aztec diamond during shuffling, there is an understanding of how the Arctic circle is occurring. When expanding the order of the Aztec diamond, the dominoes move in the direction of the arrow. At the boundaries, the dominoes can slide either east and west, or north and south. Consider the tiling as seen in Figure 9 - if the dominoes move in the latter direction, there remains a two-by-two block for establishing new dominoes. This set will have a 50% chance of either facing the north and south again, or

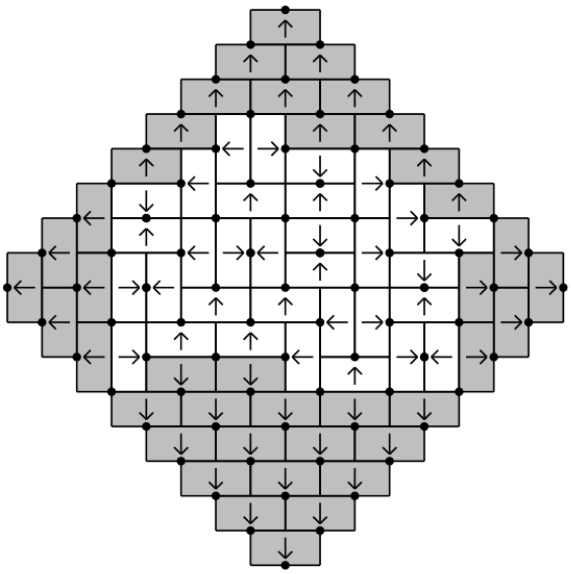

(A) Domino tiling $A_8$ about to pass through the stages of the shuffling algorithm.

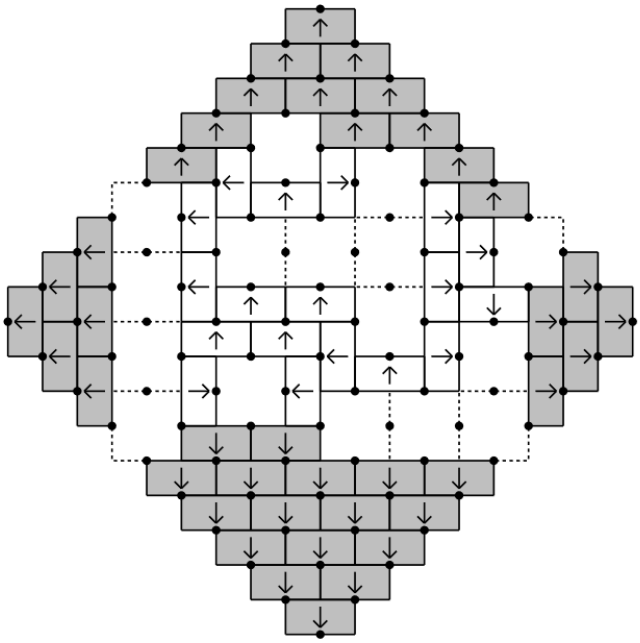

(B) The Domino tiling $A_8$ has been expanded into a domino tiling of $A_9$ through the shuffling algorithm.

FIGURE 9. Expansion of $A_8$ to $A_9$ by utilising the shuffling algorithm. The bad blocks were removed, and the remaining dominoes were shifted in the direction of their corresponding arrow. Gaps remain, where good blocks will be created [**10**].

in the east and west direction. When the domino slides into the west direction, the domino remains even if there is an infinite expansion of the order; hence, giving the frozen region.

CHAPTER 3

# The Random Assignment Problem and Belief Propagation

## 1. The Assignment Problem

Considering the commonly applied combinatorial optimisation process for finding the Maximum Weight Matching in a bipartite graph, which will be referred to as the Assignment Problem (AP) [**3**] [**2**] [**17**]. The classical representation for the AP is to consider $N$ workers and $N$ jobs, where each worker $i$ has been assigned a cost for completing job $j$. The idea is to find a way to minimise the cost for the project in such a way that each worker $i$ has a job $j$ in a bijective manner.

1.0.1. *Mathematical formulation.*

To put into a mathematical perspective by considering a weighted undirected complete bipartite graph $K_{N,N} = (\mathcal{V}_1, \mathcal{V}_2, \mathcal{E})$, where $\mathcal{V}_1 = \{1, ..., N\}$ and $\mathcal{V}_2 = \{1, ..., N\}$, and $\{i, j\} \in \mathcal{E}$ where $i \in \mathcal{V}_1$ and $j \in \mathcal{V}_2$ and for $1 \leq i, j \leq n$. Let each edge $(i, j)$ have weight $w_{ij} \in \mathbb{R}^+$. Here

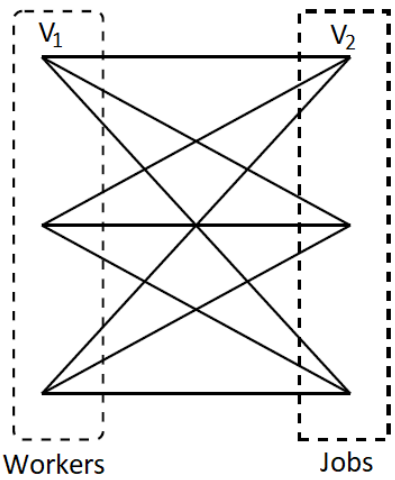


(A) Graphical representation of the Assignment problem with 3 workers and 3 jobs.

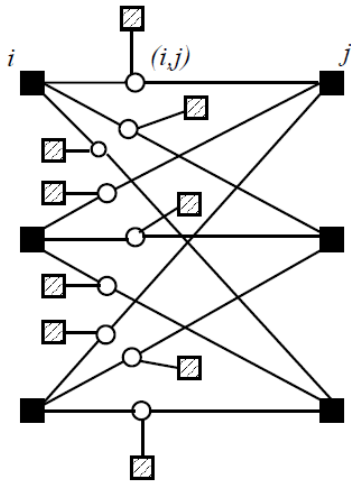


(B) Factor graph representation of the same Assignment problem, where the dashed filled squares are the functional nodes that hold the edge weights.

FIGURE 1. A small Assignment problem represented in (A) being viewed as a factor graph in (B). Every edge holds a cost, and the solution results in a perfect matching such that there are only 3 edges which are vertex disjoint, and the sum of their costs is minimal [**17**].

there would be an $N \times N$ cost matrix $\{E_{ij}\}$ given that $|\mathcal{V}_1| = |\mathcal{V}_2| = N$. An assignment is such that each node $i$ is only connected to one node $j$, following the variable for the occupancy number $m_{ij} \in \{0, 1\}$, where $m_{ij} = 1$ if the edge exists, and $m_{ij} = 0$ otherwise. Following the constraint

$$\sum_{i \in \mathcal{V}_1} m_{ij} \leq 1 \qquad \forall j \in \mathcal{V}_2, \tag{6}$$

$$\sum_{j \in \mathcal{V}_2} m_{ij} \leq 1 \qquad \forall i \in \mathcal{V}_1, \tag{7}$$

such that the assignment is a bijective matching from nodes $\mathcal{V}_1$ to nodes $\mathcal{V}_2$, and therefore it is the permutation of the set $\pi$ of $\{1, ..., N\}$ [**20**] [**17**]. A matching is defined as a set of non-adjacent edges, such that any edge has no node in common. Therefore, a maximal matching is when having an additional edge to a current matching would mean that the graph is no longer matching. A matching is maximum when the graph has maximal cardinality with the maximal matching. Finally, since a perfect matching is a matching that matches all nodes of the graph, then evidently by following these definitions, a perfect matching must be maximal and maximum [**17**]; hence, it is possible to search for the maximum cardinality matching that has a minimum cost with the above equations, and thus maximised by using

$$|M| = \sum_{ij} m_{ij}, \tag{8}$$

and the cost of the matching is given by

$$E_{K_{N,N}}[M] = \frac{1}{|M|} \sum_{ij} m_{ij} w_{ij}, \tag{9}$$

such that the optimisation is finding the permutation that minimises $E_{K_{N,N}}[M]$ [**20**].

1.0.2. *Average Optimal Cost.*

The interest in the minimum-weight perfect matching for a bipartite graph with $N$ vertices to $N$ vertices, and the behaviour of the Average Optimal Cost (AOC) was evaluated using both the replica approach, and the cavity method for $N \to \infty$. The vertices were weighted by edges with i.i.d random variables from an exponential distribution.

It was discovered that when $N \to \infty$, the AOC followed the conjuncture

$$\sum_{i=1}^{N} \frac{1}{i^2}, \tag{10}$$

and evidently, the AOC converges at $\pi^2/6$ [**20**] [**18**].

Such a conjecture proves useful for the AP, as the AOC can be used as a method to prove that weights are indeed random, and for $N$ of any size the AOC will converge.

### 1.1. Belief Propagation Algorithm.

Belief propagation (BP) or max-product is an iterative message-passing algorithm used for performing inference of a discrete probability distribution specified by a graphical model [**3**] [**2**] [**17**]. Such a method is often used to accurately compute the marginal distribution of a graphical model for each variable, and the conditional probability distribution of any variable - or additionally to find the maximisation, such that finding the most probable state in which the graphical model would obtain is desirable. Normally, it would otherwise take a

naive method of solving by summing all configurations in a graphical model with N variables $\underline{x} = (x_1, ..., x_N)$ - evidently this method would grow exponentially. The complexity of this method can be reduced by utilising BP which recursively sums over all variables, such that BP can been proved to converge to the optimal solution in polynomial time.

The development of BP has been proven to be highly efficient in tree-graphs, such that it can compute marginals and partition functions correctly; however, it may be considered naive to assume that BP can be used for general graphs, such as graphs that contain cycles, or loops. The use of Loopy Belief Propagation (LBP) has been used on graphs containing loops, but does not guarantee convergence, and computed marginals are often approximations. However, some cases have shown that LBP can be used under specific conditions to solve regular graphs with extreme accuracy [**17**].

1.1.1. *Message Passing.*

Consider the graph found in Figure 2 with three variable nodes and three functional nodes, written as the function [**16**]

$$g(x_1, x_2, x_3) = f_A(x_1) f_B(x_1, x_2) f_C(x_2, x_3), \tag{11}$$

where $x_1, x_2, x_3 \in \{1, 2, ..., N\}$, is used to efficiently compute

$$g_1(x_1) = \sum_{x_2, x_3} g(x_1, x_2, x_3). \tag{12}$$

The sums in the equation (11) can be regrouped in terms of messages between variable nodes and factor nodes [**16**] [**17**]. This is achieved by recursively pushing the summation, where for $g_1(x_1)$ messages are first sent from the furthest node towards the parent node, such that the first message is sent from variable node $x_3$ to factor involving $x_2$ and $x_3$:

$$\sum_{x_2, x_3} g(x_1, x_2, x_3) = f_A(x_1) \sum_{x_2} f_B(x_1, x_2) \sum_{x_3} f_C(x_2, x_3), \tag{13}$$

where the last summation can be reduced as a message passed from right to left where

$$\sum_{x_3} f_C(x_2, x_3) = \mu_{f_C \to x_2}(x_2). \tag{14}$$

This reduces the equation to

$$\sum_{x_2, x_3} g(x_1, x_2, x_3) = f_A(x_1) \sum_{x_2} f_B(x_1, x_2) \mu_{f_C \to x_2}(x_2). \tag{15}$$

Again, the last summation is reduced as a message passed, where

$$\sum_{x_2} f_B(x_1, x_2) \mu_{f_C \to x_2}(x_2) = \mu_{f_B \to x_1}(x_1), \tag{16}$$

and thus giving

$$g_1(x_1) = f_A(x_1) \mu_{f_B \to x_1}(x_1), \tag{17}$$

which is far more efficient than equation 12.

Understanding this relation can show that there is a large reduction in calculations necessary to solve equation 1.1.1, especially in regards to large graphs. For example, if there were a function

$$g(x_1, x_2, ..., x_k) = f_2(x_1, x_2) f_3(x_2, x_3) ... f_k(x_{k-1}, x_k), \tag{18}$$

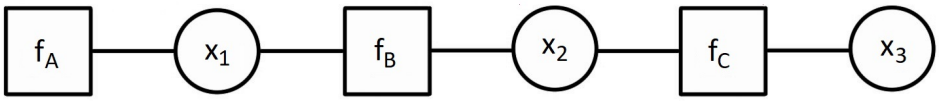


FIGURE 2. Graphical representation of equation (11), where the circular nodes represent variable nodes, and the square nodes represent functional nodes.

where $x_1, x_2, ..., x_k \in \{1, 2, ..., N\}$, to compute

$$g_1 = \sum_{x_2, x_3, ..., x_k} g(x_1, x_2, ..., x_k), \tag{19}$$

without message-passing, there would be one summation over $k-1$ variables resulting in $O(N^k)$ calculations; whereas, by utilising message-passing, there would be $k-1$ summations over one variable giving $O(k \times N^2)$ calculations, which is significantly less in larger graphs.

Following the example from above, the message-passing update rules for BP in factor graphs can be generalised, where for each edge $(i, a)$ there is a factor node $i$ and a variable node $a$. These messages are iteratively computed (where $t$ stands for the $t$-th iteration) locally at the nodes; therefore, the nodes are updating the outgoing messages depending on the incoming messages. These update rules for BP [**17**] are as follows:

$$\mu_{j \to a}^{(t+1)}(x_j) \cong \prod_{k \in \partial j \setminus a} \hat{\mu}_{b \to j}^{(t)}(x_j), \tag{20}$$

$$\hat{\mu}_{a \to j}^{(t)}(x_j) \cong \sum_{\underline{x}_{\partial a \setminus j}} \psi_a(\underline{x}_{\partial a}) \prod_{k \in \partial a \setminus j} \mu_{k \to a}^{(t)}(x_k), \tag{21}$$

where $\partial j \setminus a$ means in the neighbourhood of node $j$ except for node $a$, and $\psi$ is a parity check function.

It is important to note that the above are normalised distributions and therefore writing the partition function $Z$ explicitly is negated by using $\cong$ to denote that the BP equations conform to equality up to a normalisation. Additionally, when $\partial j \setminus a$ is an empty set, then $\mu_{j \to a} = \frac{1}{|X|}$ and when $\partial a \setminus$ is empty, then $\hat{\mu}_{a \to j} = \psi_a(x_j)$.

After the final iteration, BP estimates the marginal distribution for variable $i$ is given from the set of all incoming messages and the BP estimate is finally given as

$$\mu_i^{(t)}(x_i) \cong \prod_{a \in \partial i} \hat{\mu}_{a \to i}^{(t-1)}(x_i). \tag{22}$$

The benefit of BP over other message-passing algorithms is that it computes exact marginals on tree-graphs. Considering a complete bipartite graph, as described in section 1.0.1, passing messages through this graph would loop. However, despite the loops, BP can be used to compute the marginals exactly on such a graph.

1.1.2. *The Ising Model.*

As an example of BP, consider the one-dimensional Ising model [**17**]. The variables are Ising spins $\underline{\sigma} = (\sigma_1, ..., \sigma_N)$, where each site is associated with a random variable given the value of

either +1 for spin-up or -1 for spin-down. Their joint distribution takes the Boltzmann form as

$$\mathbb{P}(\underline{\sigma}) = \frac{1}{Z} exp\left\{-\beta E(\underline{\sigma})\right\},\ E(\underline{\sigma}) = -\sum_{i=1}^{N-1} \sigma_i \sigma_{i+1} - B\sum_{i=1}^{N} \sigma_i. \tag{23}$$

To compute the marginal probability distribution, three incoming messages towards the corresponding node are used, which represent their contribution to the marginal probability distribution. Therefore, these are defined as

$$\hat{\mu}_{j\leftarrow}(\sigma_j) = \frac{1}{Z_{j\leftarrow}} \sum_{\sigma_{j+1}\ldots\sigma_N} exp\left\{\beta \sum_{i=j}^{N-1} \sigma_i \sigma_{i+1} + \beta B \sum_{i=j+1}^{N} \sigma_i\right\}, \tag{24}$$

$$\hat{\mu}_{\rightarrow j}(\sigma_j) = \frac{1}{Z_{\rightarrow j}} \sum_{\sigma_1\ldots\sigma_{j-1}} exp\left\{\beta \sum_{i=1}^{j-1} \sigma_i \sigma_{i+1} + \beta B \sum_{i=1}^{j-1} \sigma_i\right\}. \tag{25}$$

Since these messages are probability distributions, and understanding that they are to be normalised, $Z_{\rightarrow j}$ and $Z_{j\leftarrow}$ are set by the conditions $\hat{\mu}_{\rightarrow j}(+1) + \hat{\mu}_{\rightarrow j}(-1) = 1$ and $\hat{\mu}_{j\leftarrow}(+1) + \hat{\mu}_{j\leftarrow}(-1) = 1$. Therefore, like previously, $\cong$ is used to mean that there is equality up to the normalisation. Therefore, by rearranging the summations over the spins, the marginal probability distribution can be written as

$$\mathbb{P}(\underline{\sigma}) \cong \hat{\mu}_{\rightarrow j}(\sigma_j) e^{\beta\sigma_j} \hat{\mu}_{j\leftarrow}(\sigma_j). \tag{26}$$

Each factor in this equation is a message sent to $j$ from the functional nodes that are connected to variable $j$, where each message coincides with the marginal distribution of $\sigma_j$, and therefore each neighbouring node to $j$ is the distribution of all prior messages from it's neighbour. The decomposition of this behaviour means that the messages can be computed iteratively, and allows all marginals $\mathbb{P}(\sigma_j)$ to be computed in linear time.

### 1.2. Applying Belief Propagation on the Assignment Problem.

The application of BP on AP closely follows the general message passing rules previously discussed [**17**] [**3**] [**2**]. Note that node $i$ corresponds to set $\mathcal{V}_1$, and node $j$ corresponds to set $\mathcal{V}_2$. Therefore it can be explicitly written, that the equation for updating messages in the Assignment problem is:

$$\mu^{i\rightarrow e}(m_e) \propto \sum_{\substack{m_e \\ \hat{e}\neq e}} \mathbb{I}\left(m_e + \sum_{\hat{e}\rightarrow i} m_{\hat{e}} \leq 1\right) \prod_{\substack{\hat{e}\rightarrow i \\ \hat{e}=(k,i)\neq e}} \mu_{\hat{e}\rightarrow j}(m_{\hat{e}}), \tag{27}$$

$$\mu^{e\rightarrow i}(m_e) \propto \hat{\mu}_{j\rightarrow e}(m_e) e^{-\beta m_e (w_e - 2\gamma)}, \tag{28}$$

where $\mathbb{I}(s)$ is the indicator function, and is such that $\mathbb{I}(s) = 1$ if $s$ is true, and zero otherwise. These equations from subset $\mathcal{V}_1$ to $\mathcal{V}_2$ can be inverted to receive messages from subset $\mathcal{V}_2$ to $\mathcal{V}_1$. The introduction of a cavity field $h^{i\rightarrow e}$ that parametrises the message $\mu^{i\rightarrow e}(m_e)$ is possible since variables $m_e$ take a value of either 0, or 1, and can therefore be parametrised by a single real number [**17**] [**20**], giving

$$h^{i\rightarrow j} = \gamma + \frac{1}{\beta} ln \frac{\mu^{i\rightarrow e}(0)}{\mu^{i\rightarrow e}(1)}, \tag{29}$$

$$h^{j\to i} = \gamma + \frac{1}{\beta} ln \frac{\mu^{j\to e}(0)}{\mu^{j\to e}(1)}, \tag{30}$$

$$h^{i\to j} = -\frac{1}{\beta} ln[e^{-\beta\gamma} + \sum_{\hat{e}\to i} e^{-\beta(w_{\hat{e}} + h^{k\to j})}], \tag{31}$$

$$h^{j\to i} = -\frac{1}{\beta} ln[e^{-\beta\gamma} + \sum_{\hat{e}\to i} e^{-\beta(w_{\hat{e}} + h^{k\to i})}]. \tag{32}$$

Therefore the marginal distribution of the variable $m_e$ is parametrised as

$$\mu(m_e) \propto exp[-\beta(w_e - h^{i\to e} - h^{j\to e})m_e], \tag{33}$$

and for when $\beta \to +\infty$ and $\gamma \to +\infty$:

$$h^{i\to e} = \min_{\substack{\hat{e}\to i \\ \hat{e}=(k,i)\neq e}} (w_e - h^{k\to \hat{e}}). \tag{34}$$

Notice that $e^{-\gamma}$ is a soft constraint, and when $\gamma \to \infty$, the distribution concentrates on perfect matching. When $\beta \to \infty$, the distribution concentrates on the minimal cost assignment. Therefore, recovering the ground state of the optimisation problem in the double limit with $\gamma \to \infty$ and then $\beta \to \infty$. Finally, node i is matched using edge $\hat{e}$ in either two ways, where

$$e^* = \arg \min_{\substack{\hat{e}\to i \\ \hat{e}=(k,i)\neq e}} (w_e - h^{k\to \hat{e}}), \tag{35}$$

or equivalently, the edge $e = (i, j)$ is occupied if

$$w_e \leq h^{i\to e} + h^{j\to e}. \tag{36}$$

Using this method, the equation can be used to solve a specific instance of the problem by utilising BP message-passing. The programmatic structure for BP in the Assignment problem has been previously structured in references [**2**][**3**]; therefore, already giving a foundation for the algorithm to be written.

As previously stated, it has been proven that BP can solve marginals in tree-graphs exactly, though it is no secret that the AP is not locally tree like. However, BP has been proven by contradiction to converge to an optimal solution in polynomial time. Thus, BP has been used to compute the optimal configuration in the AP using the replica symmetric cavity method.

A short analysis on this projects application of BP on the Aztec diamond, and the efficiency is given in Appendix A.

CHAPTER 4

# Frozen region on the randomly weighted Aztec diamond

## 1. The Partition Function

A uniform tiling measure is such that all tilings are equally weighted. Now consider the Random Dimer Model (RDM), where the given graph, $\mathcal{G}(\mathcal{V}, \mathcal{E})$, is such that the vertex set is given as $|\mathcal{V}| = 2N$ and the edge set is given as $\mathcal{E} \subset \mathcal{V} \times \mathcal{V}$. Each edge $e$ is associated to a weight $w_e$. It is assumed that all $w_e$ to be i.i.d. with distribution

$$\rho(w) = \exp[-w]. \tag{37}$$

Each covering is assigned a cost $E[\mathcal{D}]$:

$$E[\mathcal{D}] = \sum_{e \in \mathcal{D}} w_e. \tag{38}$$

Then, a probability proportional to the *Gibbs weight* $e^{-\beta E[\mathcal{D}]}$ is associated to $\mathcal{D}$ so that the partition function is introduced as

$$Z(\beta) = \sum_{\mathcal{D}} e^{-\beta E[\mathcal{D}]}. \tag{39}$$

Therefore, $Z(\beta)$ is the partition function of the probability distribution of the dimers, and where $\beta$ is the inverse temperature. By setting $\beta \to 0$, all dimer coverings have the same weight. This of course means that the partition function $Z(0)$ is the number of all possible dimer coverings on graph $\mathcal{G}$ [**6**].

The assumption taken is that the weights $w_e$ are identically distributed random variables with a continuous probability density $\rho(w)$, and also assume that more than one dimer covering is possible. The ground state is to be the optimal dimer configuration and is taken as the dimer covering $\mathcal{D}^*$ with the minimal cost as

$$E[\mathcal{D}^*] = \min_{\mathcal{D}} E[\mathcal{D}] = -\lim_{\beta \to \infty} \beta^{-1} \ln Z(\beta). \tag{40}$$

Evidently, $\beta$, though fictitious, determines the probability of the configuration outcome, and while setting $\beta$ to zero gives a uniform distribution, setting $\beta \to \infty$ gives the zero temperature limit, where the temperature $T = \frac{1}{\beta}$ - which is the ground state, and therefore the minimal costing configuration of the dimer.

## 2. The properties of the Aztec ground state

Running Belief Propagation (BP) over the randomly weighted Aztec diamond $k = 1000$ times for $n = 5, 10, 20, 30, 40$ and 50, the frequency of edge occupancy $f_e$ was stored as a vector, where for edge $e = ij$ the edge occupancy

$$m_e = \begin{cases} 1 & \text{if edge } e \text{ is occupied,} \\ 0 & \text{otherwise (i.e., } e \text{ is not occupied)} \end{cases}, \tag{41}$$

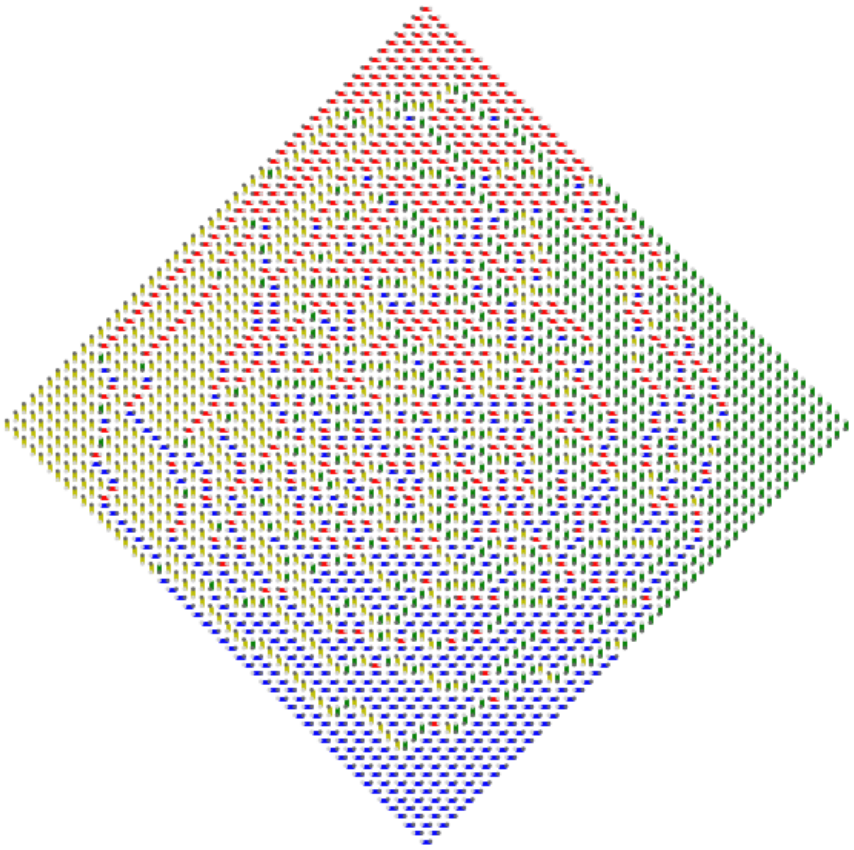

FIGURE 1. Dimer covering of the ground state of a randomly weighted Aztec diamond of order 50.

such that if an edge $e$ was occupied in instances $k$, the edge frequency $f_e = k$, and if edge $e$ was never occupied in any instance $k$, the edge frequency $f_e = 0$.

Recall that the ground state $\mathcal{D}_g^*$ is defined such that the cost of the dimer covering is the minimal cost of all possible dimer coverings, and that this optimal configuration is almost certainly unique. The use of random weights can be regarded as *noise* upon each edge of a weighted lattice.

An example of an Aztec diamond of $n = 5$, Figure 1, is a single instance of the ground state in a randomly weighted, thus unique, Aztec diamond. Notably there remains a uniform formation of edges at each corner boundary, and a higher fluctuation of the four types of dominoes towards the centre. Of course, neither Figure 1 nor an optimal dimer covering for $n$ arbitrarily large, i.e., Figure 2, would suffice in order to state the effect random weighted edges has on the Arctic region.

### 2.1. Mean and variance in the ground state.

To determine the effect of a random weighted edges on the Aztec diamond, consider the frequency of edges $f_e$ to be used to compute both the mean and variance of $e$. $f_e$ is utilised in computing the mean occupancy $\bar{m}_e$ simply by taking $\bar{m}_e = f_e/k \quad \forall e$.

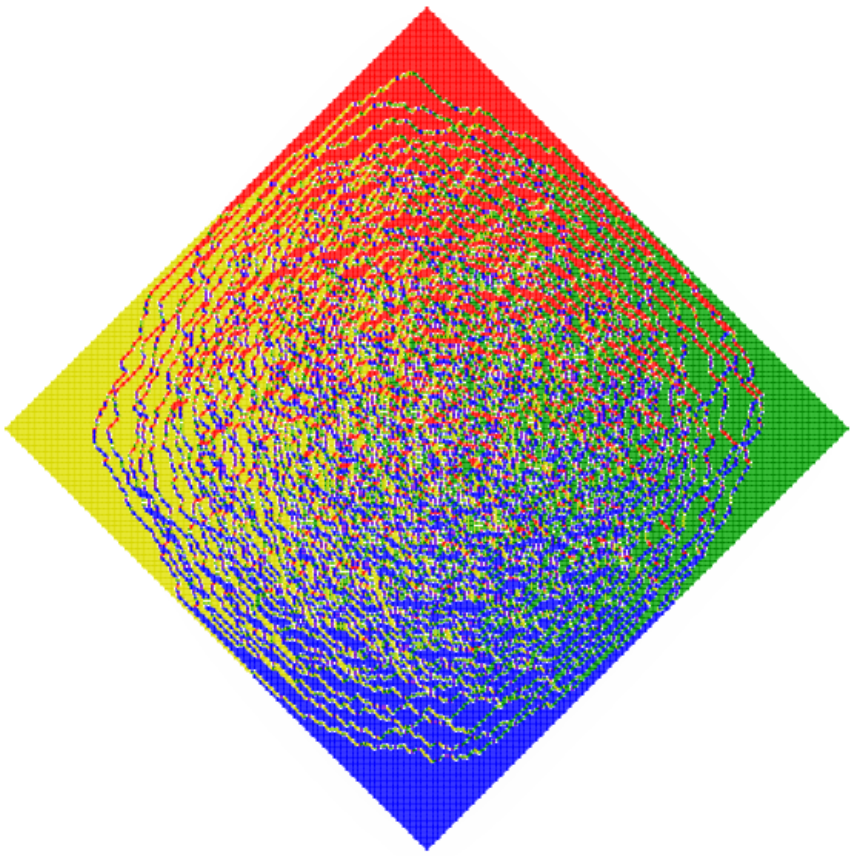

FIGURE 2. Dimer covering of the ground state of a randomly weighted Aztec diamond $n = 200$.

By replacing $f_e$ with $\bar{m}_e$, each edge is a probability measure of the edge occupancy, such that

$$\sum_{j \in \partial i} P_{ij} = 1, \tag{42}$$

meaning that for every node $j$ in the neighbourhood of node $i$, $\partial i$, there is an edge $e$ with their cumulative sum of probabilities equal to one; therefore, for every dimer covering one of these edges must be occupied. The edge probability for the ground state in the centre in Figure 3 (A) and at the boundary in Figure 3 (B) shows that the probability in the centre of the lattice leans towards edges having a uniform probability, while towards the boundary of the lattice the occupied edges become increasingly deterministic. From Figures 1 and 2, and the mean state a possibility of a phase change, the variance from $m_e$ is used to observe the limit shape on the lattice.

$$Var[e] = \frac{1}{k} \sum_{e}^{k} m_e^2 - \left( \frac{1}{k} \sum_{e}^{k} m_e \right)^2, \tag{43}$$

is used so that $Var[e] = 0$ if the edge is either always occupied or never occupied and non-zero otherwise. It is now possible to identify the effect random weights have on the Arctic region.

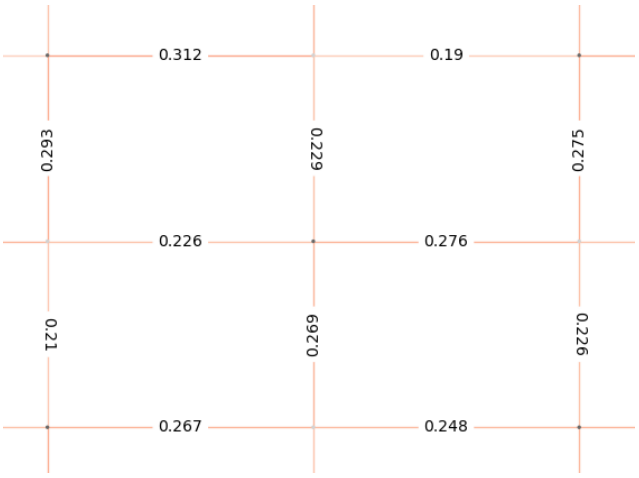


(A) Centre of the lattice.

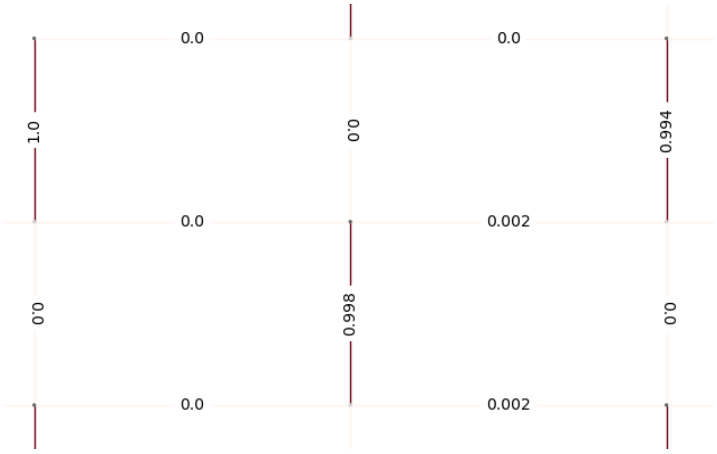


(B) Western boundary of the lattice.

FIGURE 3. Probabilities of edge occupancy at the centre and at the boundary of the Aztec diamond lattice for $n > 10$.

Figure 4 shows the variance of each edge for $n = 50$, where the green circle represents the Arctic circle with the radius of $n\sqrt{2}$ as expected when $n$ is amply large in a one-periodic weighted Aztec diamond. Evidently, the temperate region in the randomly weighted Aztec diamond seems to expand towards the boundaries more-so than what would be expected in a one-periodic weighted Aztec diamond.

Comparing the results of the variance of all edges for $n = 5, 10, 20, 30, 40,$ and 50 in Figure 5, it becomes evident that the increase of size of the randomly weighted Aztec diamond has an increase in edge variances that tend to zero, respective to the size. Establish that an edge should only be considered frozen if and only if the $Var[e] = 0$ then the frozen edges of a randomly weighted Aztec diamond are significantly smaller than the one-periodic weighted Aztec diamond, with the percentage of frozen and liquid edges given in Table 1.

Ultimately, there is evidence pointing at an increase in the Arctic region of a randomly weighted Aztec diamond as $n$ increases. However, it does not appear that it will converge to $n/\sqrt{2}$ as expected in the one-periodic weighted Aztec diamond. The limit shape of a randomly

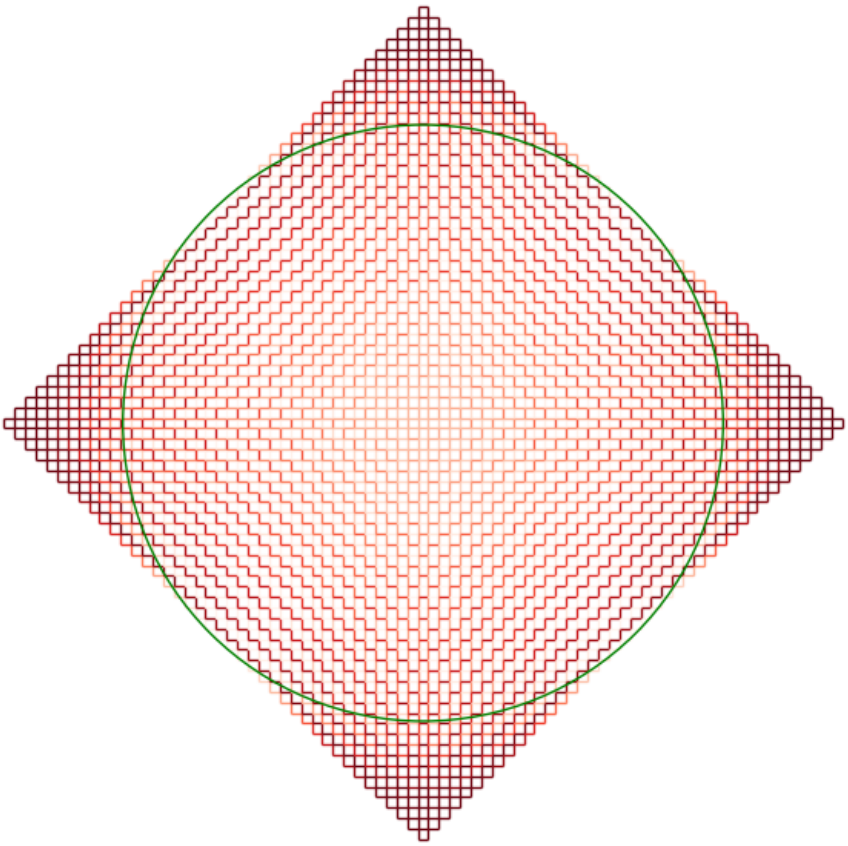

FIGURE 4. Variance of $e$ on an Aztec diamond lattice of $n = 50$, where the colour gradient represents the value of the variance, such that the darker the edge the closer the variance is to approaching zero. The green circle represents the Arctic circle found in the one-periodic weighted Aztec diamond - the radius gets arbitrarily close to $n/\sqrt{2}$ when $n$ is sufficiently large.

| **Order** | **Frozen region (%)** | **Liquid region (%)** |
|---|---|---|
| 5 | 0% | 100% |
| 10 | 0% | 100% |
| 20 | 0.1875% | 99.8125% |
| 30 | 1.11111% | 98.88889% |
| 40 | 1.59375% | 98.40625% |
| 50 | 2.19% | 97.81% |

TABLE 1. Percentages of edges considered to be frozen or liquid for various orders $n$ in the ground state.

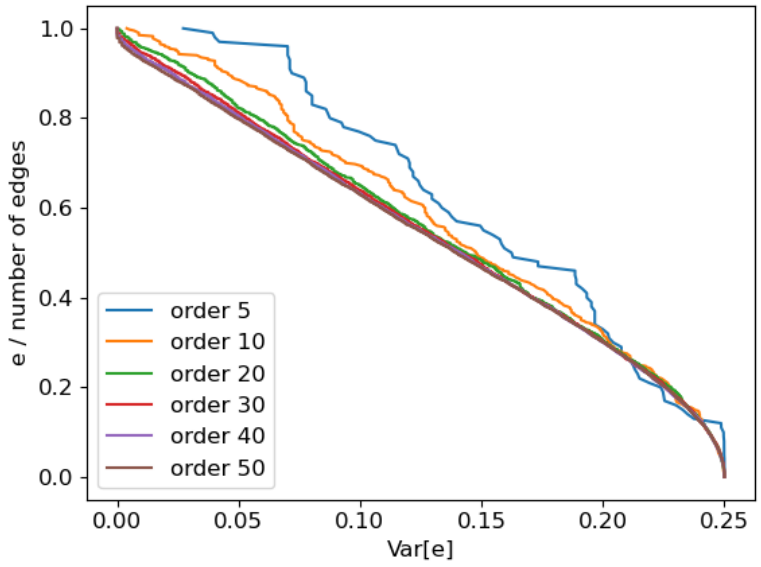


(A)

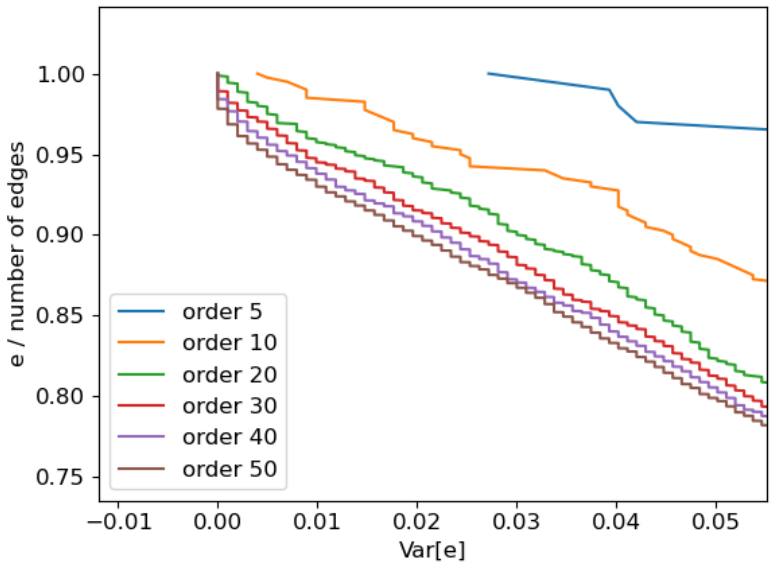


(B)

FIGURE 5. Variance of cumulative Aztec diamonds of different orders in the ground state. (B) focuses on the variance close to zero.

weighted Aztec diamond in the ground state is most certainly distorted by some variation of noise $\epsilon$. The impact of $\epsilon$ seems to give a uniform growth of the Arctic circle, where the structure and size of the Arctic regions at each polar cardinal direction are indistinguishable

from one another - therefore, the randomly weighted Aztec diamond does contain an Arctic region.

**2.2. Excitations.**
An excitation may be caused on the optimal configuration $\mathcal{D}_g^*$ by taking an edge $\hat{e}$ that occurs in $\mathcal{D}_g^*$ and either cutting $\hat{e}$, or by increasing the weight $w_{\hat{e}}$ to ensure that it could not occur in the ground state.

Since there are two areas of interest in the ground state of the Aztec diamond, the Arctic region and the Arctic circle, two separate excitations are induced in retrospect to their phases to obtain two new optimal configurations:

(1) An excitation in the liquid region gives a new optimal configuration $\mathcal{D}_l^*$,
(2) and an excitation in the frozen region gives a new optimal configuration $\mathcal{D}_f^*$,

in which both optimal configurations of the excitations $\mathcal{D}_f^*$ and $\mathcal{D}_l^*$ are of a higher cost with respect to $\mathcal{D}_g^*$. The difference between the cost significantly depends on the location of the excitation, and it is expected that $\mathcal{D}_f^*$ tends to have a higher cost than $\mathcal{D}_l^*$ as an excitation in the Arctic region would disrupt the deterministic behaviour of the dimer covering, i.e., Figure 6.

2.2.1. *Path of the excitations.*
The excitations cause self-avoiding single cycles with varying excitation lengths $s_r$, where $r$ is the region in which the excitation occurs, is evaluated by isolating the edges effected by the excitation through the symmetric difference between the ground state and the excited state, where

$$S_l = \{e \in \mathcal{E} : \mathcal{D}_g^* \triangle \mathcal{D}_l^*\}, \quad s_l = \frac{|S_l|}{2}, \tag{44}$$

$$S_f = \{e \in \mathcal{E} : \mathcal{D}_g^* \triangle \mathcal{D}_f^*\}, \quad s_f = \frac{|S_f|}{2}, \tag{45}$$

and so $\hat{e} \in S_l$ is for the excitation caused in the Arctic circle and $\hat{e} \in S_f$ is for the excitation caused in the Arctic region.

An example of these cycles obtained through the excitations of the ground state $\mathcal{D}_g^*$ found in Figure 6 are shown in Figure 7. By plotting $s$ for $k$ iterations, the difference between the effect of the excitations in both regions is seen in Figure 8. The maximum path length exhibited from an excitation in the liquid region $s_l(n)$ and in the frozen region $s_f(n)$ increase with $n$, where $s_r(n)$ is shown to depend on the location of the excitation, as anticipated. The minimum length $\min s_l(n) = 2\ \forall n$, while $\min s_f(n)$ grows with a increase in $n$.

It is shown in Table 1 that for $n = 5, 10$ each edge $e$ has a non-zero variance, and therefore neither of them exhibit a frozen region. Thus, by comparing the behaviour of the curve in Figure 8 (A) and (B) for $n = 5, 10$, both sizes prove to share the value for minimum length at $s = 2$. However, though the variance at the boundaries are non-zero, they do in fact approach zero, causing $s_f(5)$, and $s_f(10)$ to almost always be larger than $s_l(5)$, and $s_l(10)$ respectively.

Moving on to Aztec diamonds of order $n = 20, 30, 40, 50$, the behaviour of $s_l(n)$ and $s_f(n)$ become progressively obvious. An excitation caused in the Arctic circle are almost assuredly producing small values for $s_l(n)$ compared to the relative size of the Aztec diamond - even for $n = 50$ they still exhibit the minimal possible length $s = 2$. Evidently, as $s$ increases, a power-law tail develops indicating that there is a critical point induced by the finite size of the system. Whereas, an excitation caused inside the Arctic region will mostly contain an arbitrarily large $s_f(n)$.

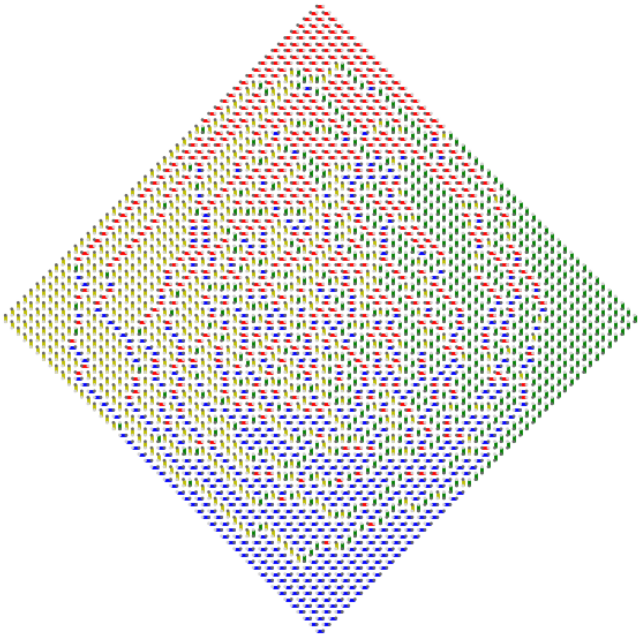

(A) Excitation caused by removing an edge with a non-zero variance towards the centre of the Aztec diamond.

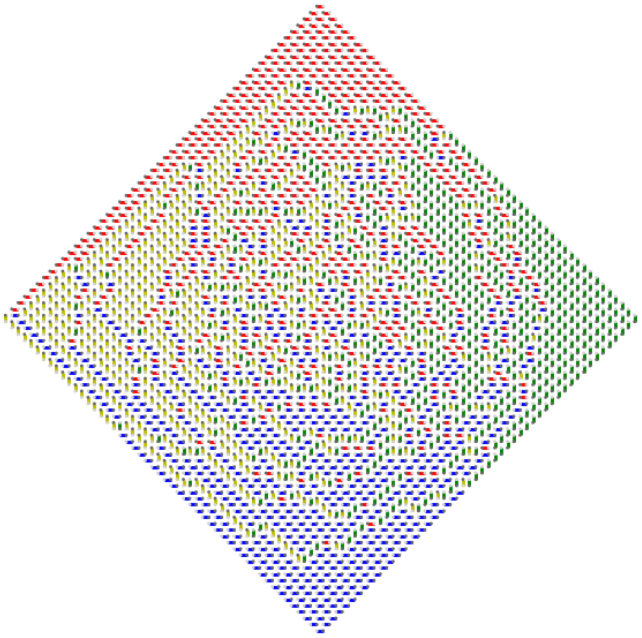

(B) Excitation caused by removing an edge with zero variance towards the boundary of the Aztec diamond.

FIGURE 6. Dimer covering of excitations caused by removing an edge either with zero variance found at the boundary of the Aztec diamond, or by removing an edge with a non-zero variance found towards the centre of the Aztec diamond.

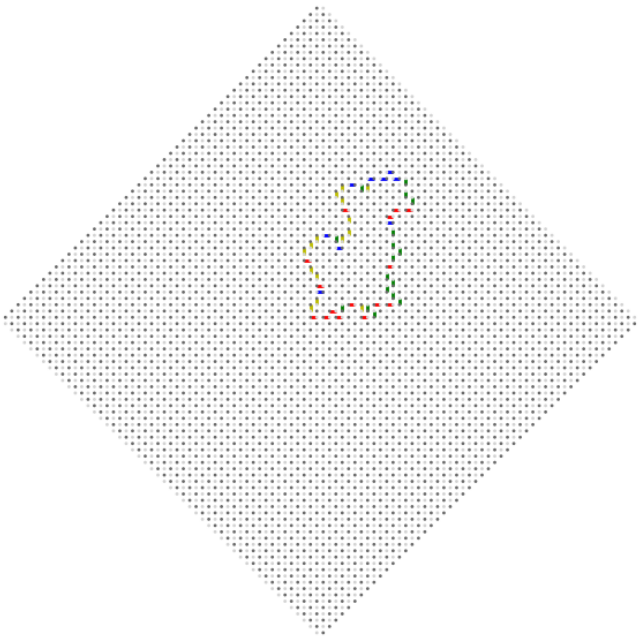

(A) Excitation in the liquid region.

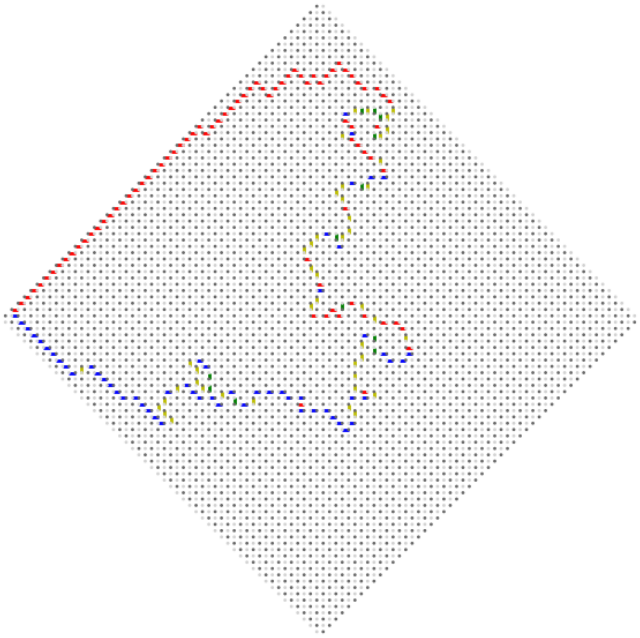

(B) Excitation in the frozen region.

FIGURE 7. Paths caused by excitations plot from the differences between $D_g^*$ and $\mathcal{D}_l^*$, and $\mathcal{D}_g^*$ and $\mathcal{D}_f^*$.

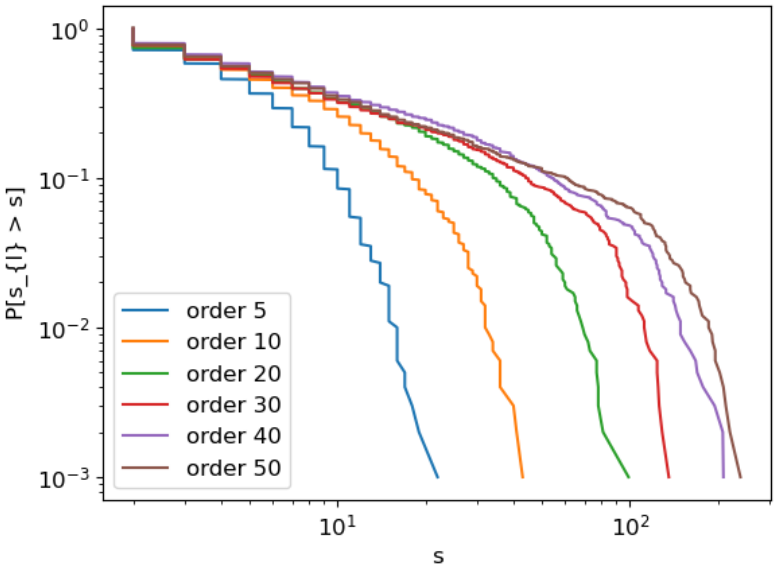


(A) Probability $\mathbb{P}[s_l > s]$.

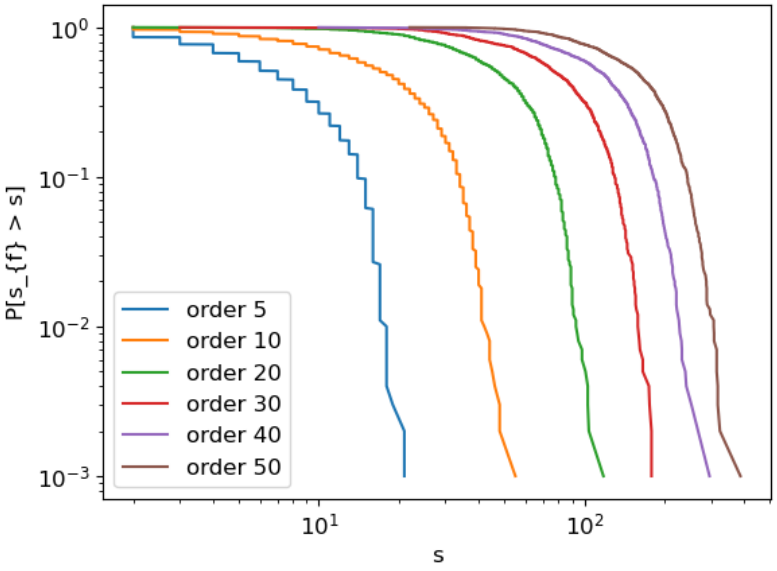


(B) Probability $\mathbb{P}[s_f > s]$.

FIGURE 8. Probability of the length of the self-avoiding single loops $s_r$ caused by excitations in the corresponding liquid and frozen region for $n = 5, 10, 20, 30, 40, 50$ in log-log.

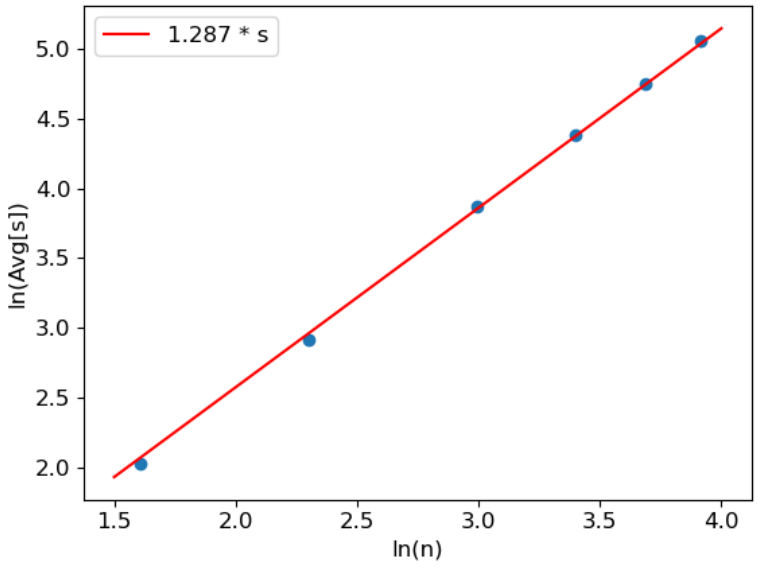


FIGURE 9. Line fitting for $\ln n$ vs. $\ln \bar{s}_f(n)$.

Given the analysis of Figure 8 (A), the probability $\mathbb{P}[s_l > s]$ can be rewritten according to scaling laws for critical systems [**6**] as

$$\mathbb{P}[s_l > s] = s^{-\zeta} g, \tag{46}$$

where $g$ is some scaling function constant for large $n$ and finite $s$. Therefore, to determine the scaling exponent $\zeta > 0$, the next step is to take the natural logarithm of equation 46, giving

$$\ln \mathbb{P} = -\zeta \ln s + \ln g, \tag{47}$$

which allows for $\mathbb{P}$ to be fit on the tail with a linear function, for $n = 50$ with $10 < s < 100$, giving a numerical estimation for $\zeta = 0.716$ and $g = 1.842$.

A different scaling behavior is observed for the excitations in the frozen region, see Figure 8 (B). Taking the natural logarithm of the size of the system $n$, and plotting against the natural logarithm $s_f(n)$ for all $n$ over $k$ iterations to get the mean path distance $\bar{s}_f(n)$, gives a scaling law in the form

$$\bar{s}_f \sim n^{\alpha}, \tag{48}$$

where $\alpha$ is the scaling exponent. A fit gives the scaling exponent as $\alpha = 1.287$, i.e., see Figure 9. With the scaling exponent $\alpha$, it is now possible to plot the cumulative distribution from Figure 8 (B) for the excitations in the frozen region by taking $s/n^{\alpha}$ vs $\mathbb{P}[s_f > s]$ in Cartesian coordinates, in Figure 10, and see that, defining $X = s_f n^{-\alpha}$, for $n$ arbitrarily large, $\mathbb{P}[X > x] \xrightarrow{n \to +\infty} \rho(x)$.

Finally, almost always, the cost of the optimal covering for the excited states abides to $E[\mathcal{D}_l^*] < E[\mathcal{D}_f^*]$, and so over $k$ iterations, for $k$ large, the average costing for $\mathcal{D}_l^*$ and $\mathcal{D}_f^*$ assuredly follows

$$\bar{E}[\mathcal{D}_g^*] < \bar{E}[\mathcal{D}_l^*] < \bar{E}[\mathcal{D}_f^*]. \tag{49}$$

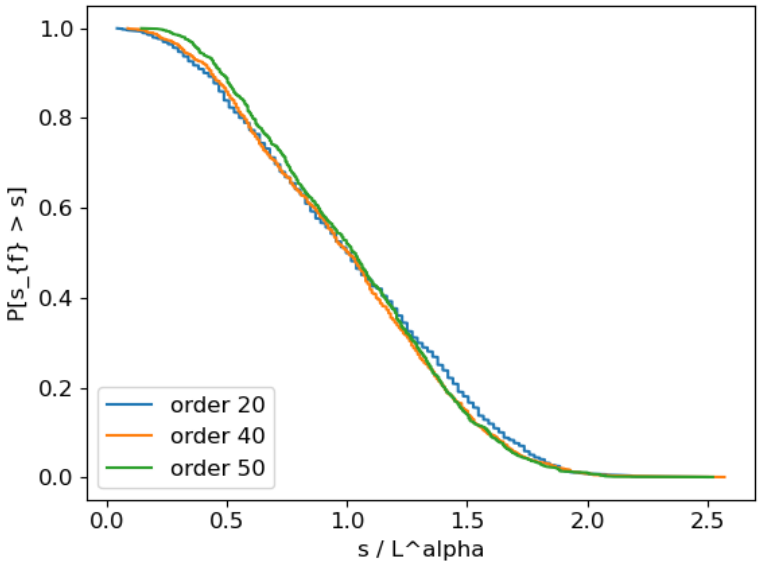


FIGURE 10. Cumulative distribution for $n = 20, 40$, and 50 after scaling.

In terms of the overall cost of the dimer covering, evidence from the data proved to show that as $n$ increases, the ratio between the mean cost of the ground state $\bar{\mathcal{D}}_g^*$ and the average cost between the excited states, $\bar{\mathcal{D}}_l^*$ and $\bar{\mathcal{D}}_f^*$, declined - suggesting that the average cost for the optimal configurations converge while following the constraint in equation 49 (the data is shown in Appendix (B)). This would indicate that the average cycle length $\bar{s}_r(n)$ does not increase at a rate ample enough to negatively impact the optimal cost in the excited states.

2.2.2. *Mean and variance of the frequency occupancy in the excitations.* Following the steps highlighted in section 2.1 in determining the mean and variance of $\mathcal{D}_g^*$, it is possible to analyse the same frequency of occupancy in the excited configurations. Explicitly, the frequency of the edge occupancy in equation (41) can be used to determine the mean and variance in the optimal dimer cover of the excited states $\mathcal{D}_l^*$ and $\mathcal{D}_f^*$.

For the excitation in liquid region, $\mathcal{D}_l^*$, it was previously stated that $s_l(n)$ occurring in the liquid region are often arbitrarily small; therefore, there is already the assumption that the cost $E[\mathcal{D}_l^*]$ will on average be a small increase on $E[\mathcal{D}_g^*]$. By removing an edge $e$ attached to node $i$ within the limit shape, the assumption would be that since any edge attached to node $i$ has an almost equal probability of occurring in the ground state, then any such edge has an almost equal probability of being cut. Therefore, $\bar{m}_e$ attached to node $i$ will still remain almost uniform after $k$ iterations of excitations, i.e., Figure 11. Since the probabilities of the edge occupancy after excitations in the liquid region remain almost equal to that of the ground state, and due to the limiting length of the excitation paths $s_l(n)$ in this region - the variance would be approximately indifferent to that in the ground state. This effect is shown in Figure 12. Hence, the variance of $\mathcal{D}_l^*$ for $k$ iterations for $n = 5, 10, 20, 30, 40$, and 50 in Figure 13.

The variance between $\mathcal{D}_g^*$ and $\mathcal{D}_l^*$ remain almost exact, while there are variance fluctuations between the edges within the limiting shape, a comparison of the variance of cumulative Aztec diamonds in the ground state shows no difference in the frozen region between the

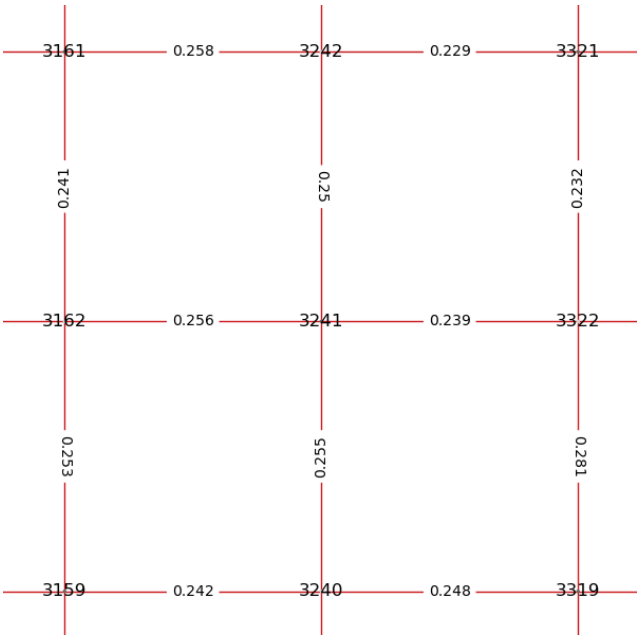


(A) Edge probabilities for the ground state.

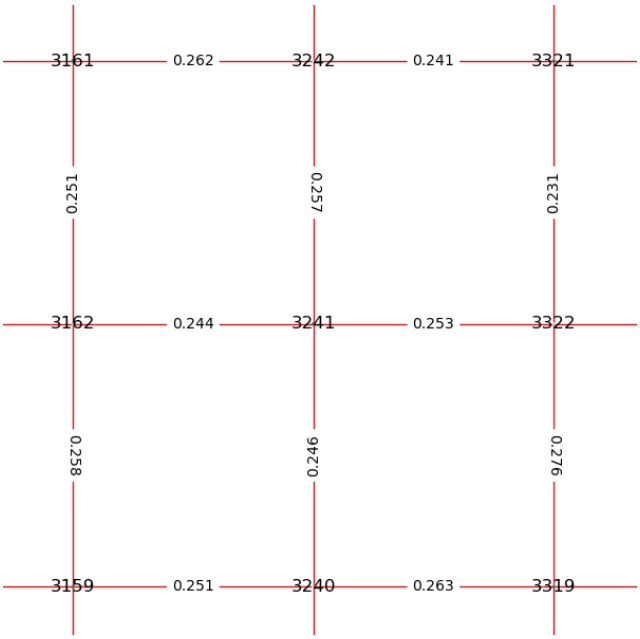


(B) Edge probabilities for the excited state in the liquid region.

FIGURE 11. Edge probabilities for edges in the neighbourhood of node $i = 3241$. Despite the introduction of excitations around node $i$, the edge probabilities remain almost equal.

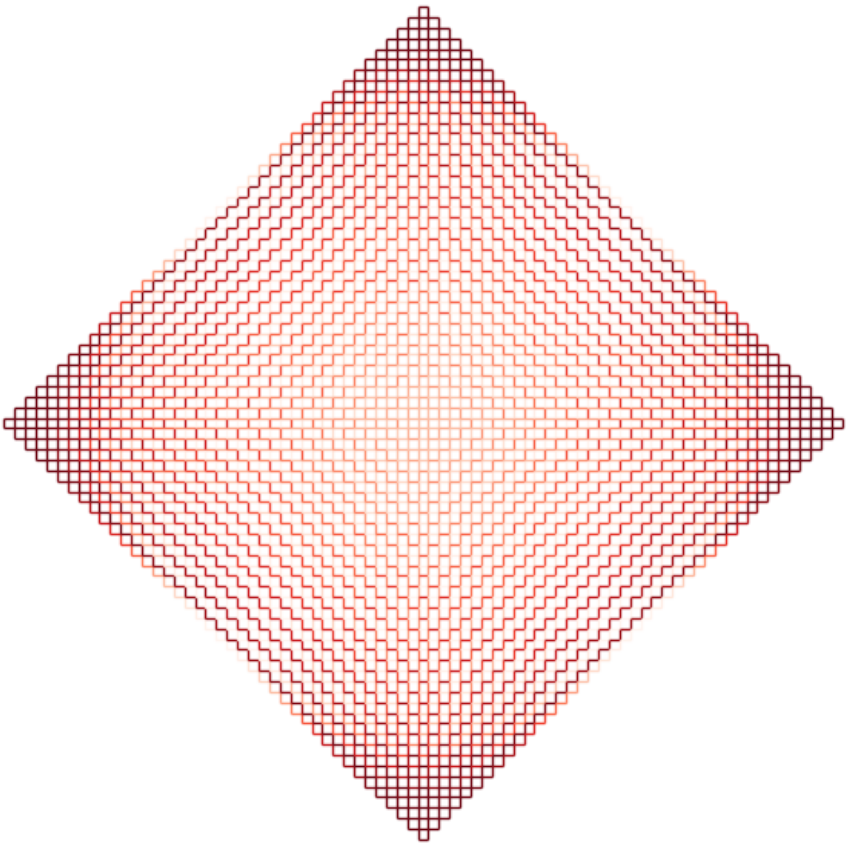

FIGURE 12. Variance of the edge occupancy frequency of order $n = 50$ after excitations were caused in the liquid region.

ground state up until $n = 40$, Table 1, and the excitations in the liquid phase shown in Table 2. For $n = 50$, there was an unexpected increase in the frozen region from an excitation caused in the liquid region. This increase is in fact extremely small, and may be considered extremely unlikely to happen or an error due to the amount of iterations $k$; therefore if $k >> 1000$ this discrepancy may disappear. It should also be considered that perhaps the excitations in the Arctic circle force the Arctic region to expand when $n \geq 50$ - perhaps this could be looked into upon further study.

The effects of excitations inside of the Arctic region for the cumulative dimer coverings of $\mathcal{D}_f^*$ run for $k$ iterations again follows the procedure explained in section 2.1. Therefore, when $k$ is sufficiently large, $\bar{E}[\mathcal{D}_f^*]$ has proven to be larger than $\bar{E}[\mathcal{D}_l^*]$ since $\bar{s}_f > \bar{s}_l$.

To understand why the cost is almost always larger, consider the mean edge occupancy in Figure 14 (A). Notably, an excitation caused at polar West will produce a path that extends at the boundary towards the polar North with certainty as $Var[e] = 0$. In fact, as the excitation is caused by removing an edge connected to a node slightly North of the polar West boundary, $s_f(n)$ for $n \geq 20$ moves towards the next closest polar cardinal point until reaching the boundary of the limit shape. The path will purposely avoid moving through the concurrent frozen region in which the excitation is located (in this case polar West), limiting

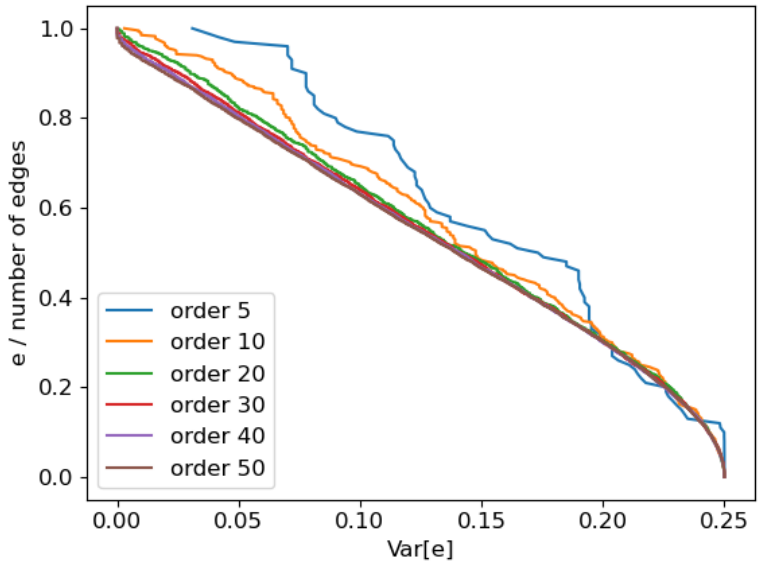


(A)

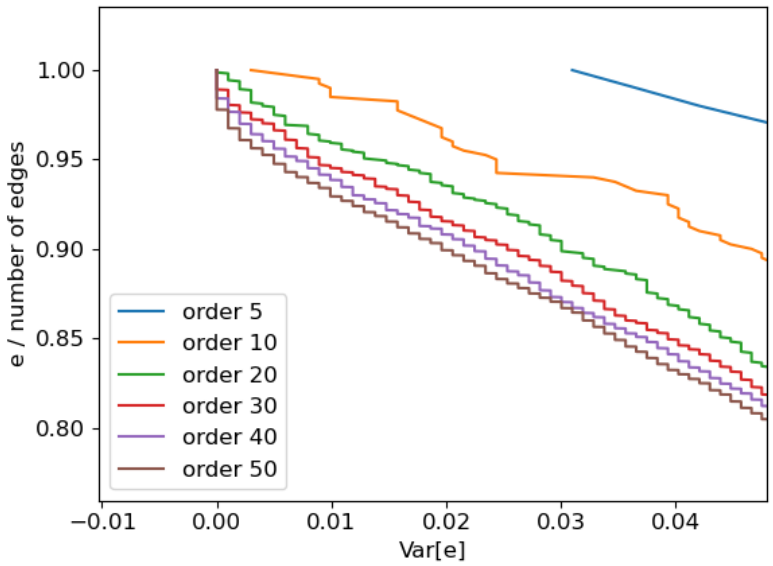


(B)

FIGURE 13. Variance of cumulative Aztec diamonds of different orders for excitations caused in the liquid region. (B) focuses on the variance close to zero.

| Order | Frozen region (%) | Liquid region (%) |
|---|---|---|
| 5 | 0% | 100% |
| 10 | 0% | 100% |
| 20 | 0.1875% | 99.8125% |
| 30 | 1.11111% | 98.88889% |
| 40 | 1.59375% | 98.40625% |
| 50 | 2.22% | 95.42% |

TABLE 2. Percentages of edges considered to be frozen or liquid for various orders $n$ after excitations in the liquid region.

| Order | Frozen region (%) | Liquid region (%) |
|---|---|---|
| 5 | 0% | 100% |
| 10 | 2.25% | 97.75% |
| 20 | 4.6875% | 95.3125% |
| 30 | 3.389% | 96.611% |
| 40 | 4.125% | 95.875% |
| 50 | 4.58% | 95.42% |

TABLE 3. Percentages of edges considered to be frozen or liquid for various orders $n$ after excitations in the frozen region.

any disruptions towards uniformly orientated edges; thus, the path towards polar South will either move at the boundary or parallel to the boundary with equal probability until reaching the liquid region - leaving a path of zero variance directly in-between them. Both paths generally end between polar North and polar South, and they join together by finding a path with minimal cost through the Arctic region with equal probability, leaving the mean edge occupancy frequency inside the Arctic circle with insignificant fluctuations. This behaviour is seen in Figure 14 (B) where the variance shows the deterministic nature of path $s_f(n)$ with $n$ arbitrarily large.

Turning to Figure 15, there most certainly is an increasing effect on the Arctic region for $10 \leq n \leq 50$. $n = 5$ would not have been expected to have developed frozen edges as the variance is more uniform across the lattice, and therefore the excitations are unbounded by any limit shape. Strangely though, both $n = 10$ and $n = 20$ have a considerable increase in frozen edges. The reason for this is not immediately evident, and this could yet be another error due to the number of iterations $k = 1000$ - though a possibility is that between the Arctic region into the Arctic circle, there is a smooth transition in the incremental increase in variance for these orders. For $n = 30, 40, 50$ the increase in the frozen region seems to have more structure than the lower orders. Table 3 shows no immediate pattern of the effect of excitations in the Arctic region; if there is any pattern that alters the size of the Arctic region, higher orders would have to be studied to formulate some composure and see that if perhaps the Arctic region will converge, or if there is merely a fluctuating increase as $n \to \infty$.

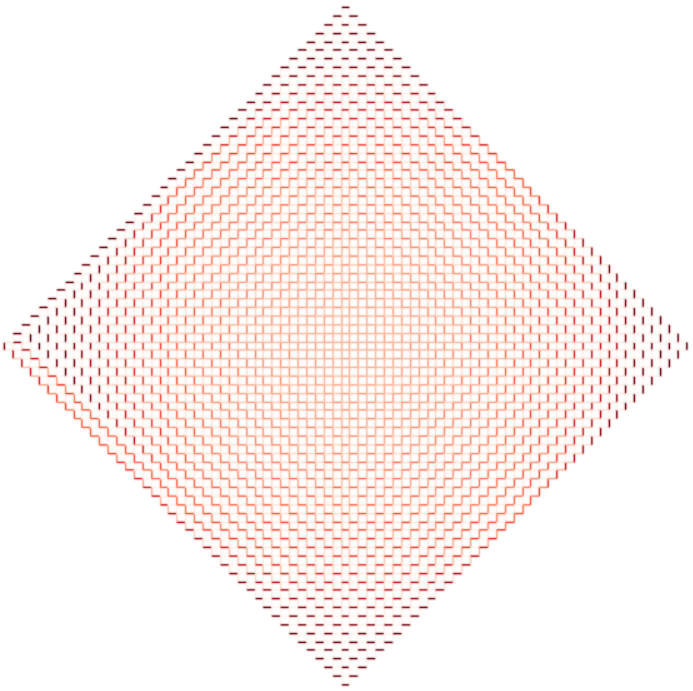

(A) Mean edge occupancy for $n = 50$.

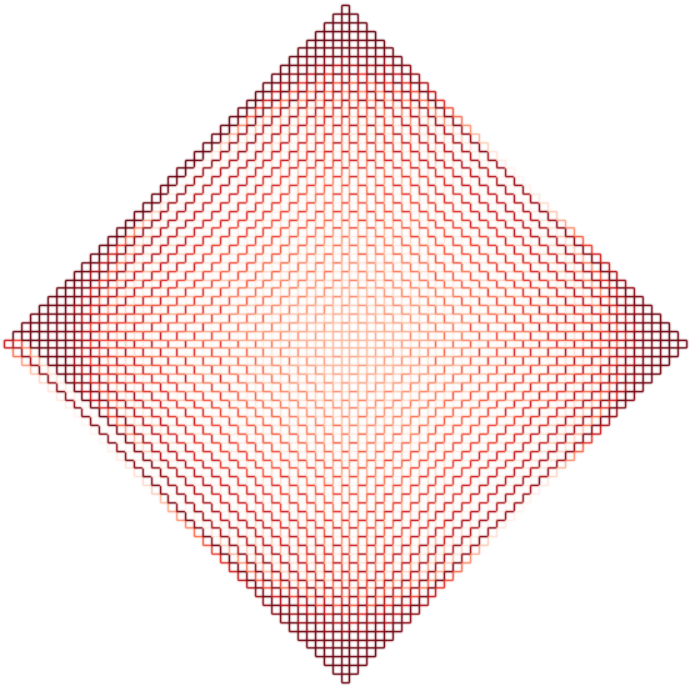

(B) Variance edge occupancy for $n = 50$.

FIGURE 14. Mean and variance of the edge occupancy frequency of order $n = 50$ after excitations were caused adjacent to the Western boundary.

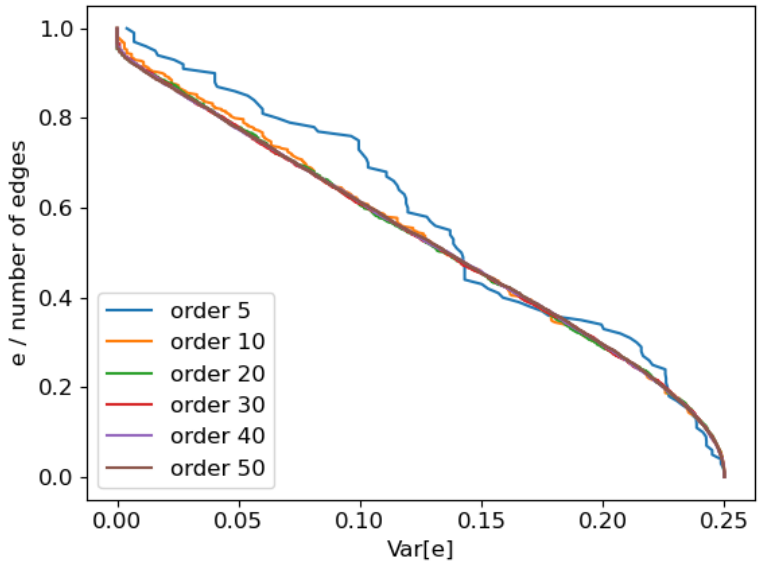


(A)

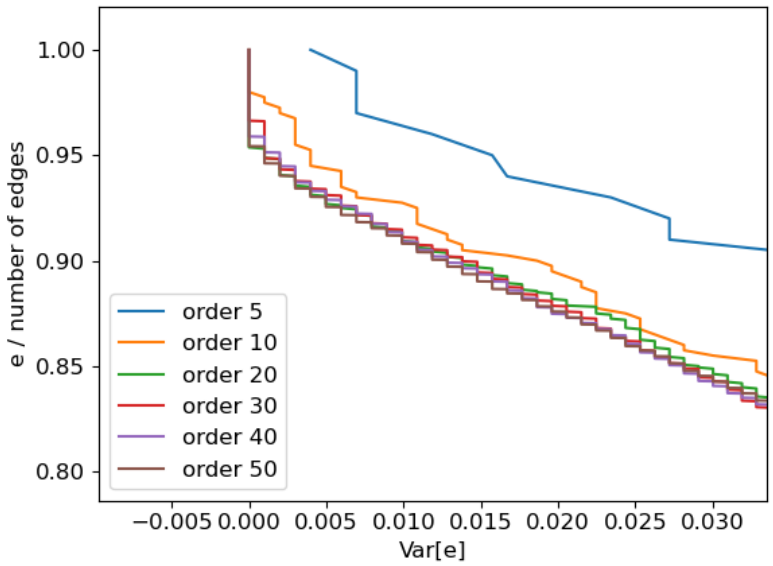


(B)

FIGURE 15. Variance of cumulative Aztec diamonds of different orders for excitations caused in the frozen region. (B) focuses on the variance close to zero.

CHAPTER 5

# Conclusions and perspectives

It has been evident for some time that the properties of dimer coverings hold considerable amount of attention, especially in statistical physics. Different approaches, or different algorithms have proven to be valuable assets. It is for this reason that this paper concentrated on using the Belief propagation (BP) on the unexplored randomly weighted Aztec diamond to analyse the unique behaviour of such a lattice.

The preliminary idea behind this paper was to take BP and apply the algorithm on the randomly weighted Aztec diamond to determine the impact on the already well documented Arctic circle. The existence of the Arctic circle became apparent in the one-periodic weighted case, and since then there have been various studies into different weighting methods on the Aztec diamond - though the randomly weighted Aztec diamond seems to be missing from the literature.

It was first proven that BP does converge to the optimal configuration on the Aztec diamond lattice in polynomial time - and at a far more efficient rate compared to that of general solvers like the one provided by Python's NetworkX. Any analysis on a randomly weighted Aztec diamond with an arbitrarily high order $n$ would otherwise have been impossible without BP.

The idea of random weights on the Aztec diamond can correspond to noise on the lattice. It was shown that in the ground state, such that the optimal configuration is that of minimum cost, the Arctic circle on the randomly weighted Aztec diamond still existed; however, it differed in terms of size compared to that of the one-period weighted Aztec diamond. The Arctic regions at the cardinal points exhibited a reduction in size; thus, as the Arctic regions became limited and the Arctic circle proved to expand towards the boundaries contorting the limit shape. However, the expanse of the limit shape proved to be structured, such that it was still uniform in appearance. The exact shape and size of the convergence of the Arctic circle on a randomly weighted Aztec diamond is yet to be shown, but leaves promise to be studied further.

Furthermore, taking the ground state of the Aztec diamond and causing excitations proved to have an effect on the Arctic region, and was dependent on the location of the excitation. The excitations would cause self-avoiding loops that would have a tendency to avoid getting close to the Arctic regions as much as possible. Excitations caused in the liquid region of the Aztec diamond would often contain very small self-avoiding loops regardless of the order $n$ - this meant that the excitations in the liquid region would have an insignificant impact on the Arctic region. As for the excitations in the frozen region, the behaviour of the self-avoiding loops showed similar characteristics as those in the liquid area, such that, the self-avoiding loops would attempt to avoid the frozen edges. To do this, one path would deterministically follow one adjoining boundary until it reached a variation in structure, the Arctic circle, while the other path would have an equal probability to follow two routes in the opposite direction at the boundary or adjacent to the boundary. These paths would then join ends by connecting though edges with minimal costing in the Arctic circle. Since one path

was deterministic, this meant that the variance of edge frequency in $k = 1000$ iterations on this path would go to zero, meaning the path was frozen. As a result, excitations caused in the Arctic region would increase the amount of frozen edges, though the Arctic circle would lose its shape.

There is certainly more to achieve in the randomly weighted Aztec diamond, and possible extensions to this paper that may be considered, such as finding out when $n \to \infty$ in a randomly weighted Aztec diamond, should the limit shape expect to converge? If so, what to? What is the relationship between the convergence of the radius of the Arctic circle in the one-periodic weighted Aztec diamond and the randomly weighted Aztec diamond? This of course would be computationally difficult, and other methods would have to be explored to find the solutions. Additionally, the data could be reconstructed for $k >> 1000$ - doing so would either alleviate possible errors, or formulate the conjuncture that the excitations in the Arctic circle may in fact impact the Arctic region for large $n$.

APPENDIX A

# Belief Propagation and NetworkX

Before studying the random dimer problem on the Aztec diamond model, a comparative study was performed between BP and Python's NetworkX algorithm for finding optimal matchings [**9**].

## 1. The NetworkX library

NetworkX is simply a Python package enabling the user to create and manipulate complex networks in order to study the dynamics and structure. Using this to first solve the AP, was used as benchmark of our BP implementation – specifically on the Aztec diamond.

NetworkX contains two algorithms that can be used to solve the Assignment problem; however, one of them can only be utilised for complete graphs. Though this functionality works perfectly well for the Assignment problem, when considering the Aztec diamond lattice, this algorithm would be inadequate. The functioning algorithm to find the ground state of both the Assignment problem and the Aztec diamond is called *max_weight_matching*. It computes the maximum-weight matching of graph $\mathcal{G}$, where the maximum-weight of the matching is the sum of all edge weights in a dimer covering. For the Assignment problem, the cardinality can be set to the max - such that, the algorithm achieves perfect matching. Based on the *blossom* method and the *primal-dual* method, and is expected to take time $O(n^3)$, where $n$ is the number of nodes [**9**].

Since the algorithm formulates the sum of all weights so that the solution is the maximum weighted graph, the weights on all edges $e$ must be inverted, either by multiplying $e$ by $-1$, or by finding the edge with the largest weight $w_e^*$ and performing the following for all edge weights $w_e$

$$w_e^* - w_e. \tag{50}$$

Both methods result in the inverted weights on the graph, thus configuring the algorithm to find the optimal costing of the graph.

## 2. Belief Propagation vs NetworkX on the Aztec Diamond

Take an Aztec diamond lattice, as described in section 1.3, of order $n$ and randomly apply weights with the exponential distribution (37), to every edge $e$. Running either the NetworkX algorithm or BP would both result in the ground state.

BP was specifically implemented for this project in Python by utilising the method structured by Bayati [**2**]. By implementing the cavity method given in Chapter 3 section 1.2, where if $w_e \geq h^{i\to e} + h^{j\to e}$ the edge is matched, BP proved to converge regardless of $n$. To grasp the sizes of the Aztec diamond lattice used, refer to Table 1.

Taking the average computation time for solving the optimal matching on the Aztec diamond via NetworkX and BP over a multitude of iterations $k$, Figure 1 displays a significant increase in computational time efficiency on a graph with $n > 10$ by utilising BP, notably as

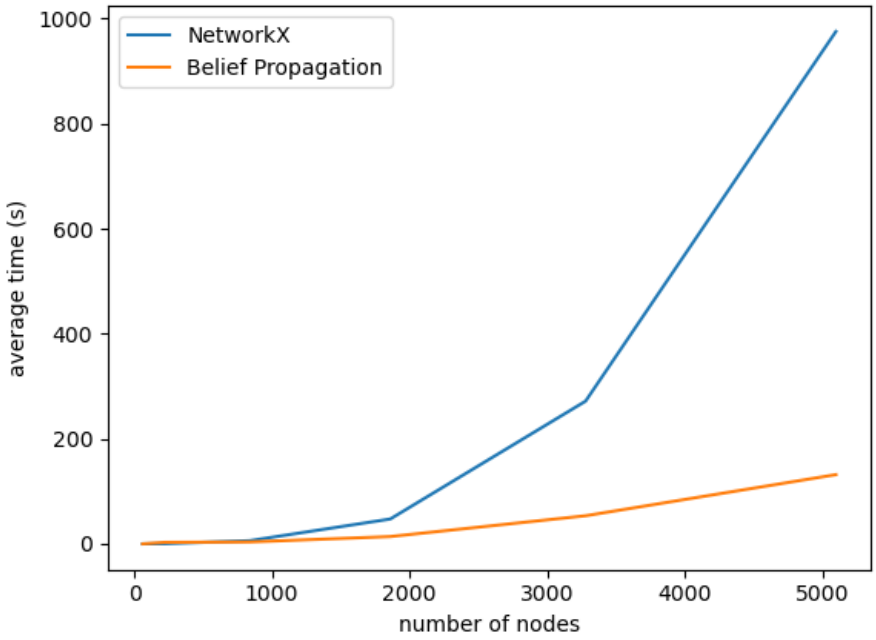


FIGURE 1. Average computational time comparison between NetworkX and BP on the Aztec diamond.

| **Order** | **no. Nodes** | **no. Total Edges** | **no. Matched Edges** | **no. Possible Coverings** |
|---|---|---|---|---|
| 5 | 60 | 100 | 30 | $= 32768$ |
| 10 | 220 | 400 | 110 | $\approx 3.60 \times 10^{16}$ |
| 20 | 840 | 1600 | 420 | $\approx 1.64 \times 10^{63}$ |
| 30 | 1860 | 3600 | 930 | $\approx 9.52 \times 10^{139}$ |
| 40 | 3280 | 6400 | 1640 | $\approx 6.99 \times 10^{246}$ |
| 50 | 5100 | 10000 | 2550 | $\approx 3.58 \times 10^{383}$ |

TABLE 1. Details of the size of the graph according to the order.

discussed in Chapter 2 section 1.1. Therefore, BP on the Aztec diamond does converge at a faster rate that NetworkX in time $t^*$, which is polynomial in the size of graph.

APPENDIX B

## Table: average cost differences between the ground state and excitations

| $n$ | $\bar{E}[\mathcal{D}_g^*]$ | $\bar{E}[\mathcal{D}_l^*]$ | $\bar{E}[\mathcal{D}_f^*]$ | $\bar{E}[\mathcal{D}_g^*]\triangle\bar{E}[\mathcal{D}_l^*](\%)$ | $\bar{E}[\mathcal{D}_g^*]\triangle\bar{E}[\mathcal{D}_f^*](\%)$ | $\bar{E}[\mathcal{D}_l^*\triangle\bar{E}[\mathcal{D}_f^*]](\%)$ |
|---|---|---|---|---|---|---|
| 5 | 18.30671 | 19.06998 | 20.37800 | 4.08417% | 10.7086% | 6.63164% |
| 10 | 67.31310 | 68.00445 | 72.14728 | 1.02182% | 6.93269% | 5.91192% |
| 20 | 257.6363 | 258.2948 | 268.8162 | 0.255236% | 4.24724% | 3.99211% |
| 30 | 569.1878 | 569.8250 | 586.6994 | 0.111897% | 3.02999% | 2.91812% |
| 40 | 1002.241 | 1002.922 | 1026.855 | 0.0679111% | 2.42608% | 2.35818% |
| 50 | 1557.971 | 1558.643 | 1589.618 | 0.0431422% | 2.0109% | 1.96776% |

TABLE 1. A comparative table between the average cost on the randomly weighted Aztec diamond in the ground state and excitations.

# Bibliography


[1] Federico Ardila and Richard P Stanley. Tilings. *arXiv preprint math/0501170*, 2005.

[2] Mohsen Bayati, Devavrat Shah, and Mayank Sharma. Maximum weight matching via max-product belief propagation. In *Proceedings. International Symposium on Information Theory, 2005. ISIT 2005.*, pages 1763–1767. IEEE, 2005.

[3] Mohsen Bayati, Devavrat Shah, and Mayank Sharma. Max-product for maximum weight matching: Convergence, correctness, and lp duality. *IEEE Transactions on information theory*, 54(3):1241–1251, 2008.

[4] Vincent Beffara, Sunil Chhita, and Kurt Johansson. Airy point process at the liquid-gas boundary. *The Annals of Probability*, 46(5):2973–3013, 2018.

[5] Kasper Borys. Domino tiling. Technical report, Department of Mathematics, The University of Chicargo, 2015.

[6] Sergio Caracciolo, Riccardo Fabbricatore, Marco Gherardi, Raffaele Marino, Giorgio Parisi, and Gabriele Sicuro. Criticality and conformality in the random dimer model. *Physical Review E*, 103(4):042127, 2021.

[7] Sunil Chhita, Kurt Johansson, and Benjamin Young. Asymptotic domino statistics in the aztec diamond. *The Annals of Applied Probability*, 25(3), Jun 2015.

[8] Henry Cohn, Richard Kenyon, and James Propp. A variational principle for domino tilings. *Journal of the American Mathematical Society*, 14(2):297–346, 2001.

[9] Aric Hagberg, Pieter Swart, and Daniel S Chult. Exploring network structure, dynamics, and function using networkx. Technical report, Los Alamos National Lab.(LANL), Los Alamos, NM (United States), 2008.

[10] William Jockusch, James Propp, and Peter Shor. Random domino tilings and the arctic circle theorem. *arXiv preprint math/9801068*, 1998.

[11] Kurt Johansson. Particle and dimer asymptotics in the aztec diamond. *http://www.birs.ca/events/2012/5-day-workshops/12w5015/videos/watch/201209240933-Johansson.html*, 07/08/2021.

[12] Pieter W Kasteleyn. The statistics of dimers on a lattice: I. the number of dimer arrangements on a quadratic lattice. *Physica*, 27(12):1209–1225, 1961.

[13] Richard Kenyon. An introduction to the dimer model. *arXiv preprint math/0310326*, 2003.

[14] Richard Kenyon. Lectures on dimers. *arXiv preprint arXiv:0910.3129*, 2009.

[15] Richard Kenyon and Andrei Okounkov. Communications-what is... a dimer? *Notices of the American Mathematical Society*, 52(3):342–343, 2005.

[16] Frank R Kschischang, Brendan J Frey, and H-A Loeliger. Factor graphs and the sum-product algorithm. *IEEE Transactions on information theory*, 47(2):498–519, 2001.

[17] Marc Mezard and Andrea Montanari. *Information, physics, and computation*. Oxford University Press, 2009.

[18] Marc Mézard and Giorgio Parisi. Replicas and optimization. *Journal de Physique Lettres*, 46(17):771–778, 1985.

[19] Do Norman. The art of tiling with rectanges. *https://users.monash.edu/ normd/documents/Mathellaneous-07.pdf*, 07/08/2021.

[20] Giorgio Parisi, Gianmarco Perrupato, and Gabriele Sicuro. Random-link matching problems on random regular graphs. *Journal of Statistical Mechanics: Theory and Experiment*, 2020(3):033301, 2020.

[21] James Propp. Dimers and dominoes. *arXiv preprint arXiv:1405.2615*, 2014.

[22] James Propp. Enumeration of tilings. *Handbook of Enumerative Combinatorics*, pages 541–588, 2014.

[23] James Propp, Noam Elkies, Greg Kuperberg, and Michael Larsen. Alternating sign matrices and domino tilings. *arXiv:math/9201305*, pages 111–132, 1992.

[24] Sherpal. Aztecdiamond. *GitHub repository, https://github.com/sherpal/AztecDiamond*, 20/08/2021.

# Self-reflection

### Guidance in the Research methods materials

**Searching for literature**. I started with the provided resources and kept comprehensive notes of all the information I thought relevant from literature and supervisor meetings. I would check the citations of relevant literature for parts I found I thought useful to expand my knowledge, i.e., the replica symmetric cavity method. I felt that this was extremely useful at times, but could also be detrimental and lead to material containing information irrelevant to the project - meaning I should have been more selective.

**Tools for doing research.** Note-keeping in general was the most important habit I kept on this project. This notebook is now a collection of information, data, and ideas - all of which I could expand upon with my supervisor. Besides the tools applied to me by KCL, such as it's library catalogue; I heavily utilised Python quite efficiently during this project. The tool I wish I did use was another graphing software - Python worked decently; however, the graphical output could have been presented better.

**Writing up and presenting your research**. The writing process was the most difficult for me. Some days I could barely get a paragraph out, and on other days the data was being tediously scaled in a way that was not presentable. These both took a lot of determination to overcome with success. I believe that through persistence I ultimately managed to write about the relevant literature, my ideas, and results clearly, as well as present my results and data extremely well.

### Marking Scheme

**Scientific quality.** I believe the majority of the relevant material in the project scope was covered. The methods in which I managed to obtain the data were all introduced in the first two chapters of the project, and then implemented for the results in chapter 4, where I could critically evaluate the results, and see that the results made sense. I even looked at the likely hood of errors in the data when something looked out of place - I discussed the most likely scenario, but also my own idea of what could be occuring if it is not an error. I believe my code became less efficient overtime - by reducing computation time for 1 iteration by 60 seconds could have saved days in computational time. This means I could have had time to study say the finite temperature limit.

**Breadth.** There are parts of this project connected to modules and lectures I had taken at KCL, such a complex networks, statistical mechanics, and many body systems; however, these modules consisted of only part of the foundation of the project. This was the first time I have ever had to create any sort of algorithm, and none of my modules were computationally heavy. When Belief propagation proved to be successful on the Aztec diamond, that was probably the most satisfying moment during the project. As for an improvement, there was certainly more I could have expanded the project to with ample time - to start, I would definitely would have like to expand the project to study the finite temperature limit.

**Originality.** The Aztec diamond has been amply studied with specifically weighted edges, however there is no literature for the randomly weighted Aztec diamond. This meant that I could take an approach that took the behaviour of the Aztec diamond on a previously studied weighting system and compare it to the randomly weighted Aztec diamond. I was fortunate to have a supervisor who had similar ideas of where the project could go and what I should do, which made the project's path smooth. I took my own initiative and decided that it would be better to analyse higher order systems for the ground state and excitations, rather than studying lower orders and then also studying the case in the finite temperature limit. The results proved valuable - but I am unsure if I made the correct choice.

**Presentation** I believe the entire report was consistently well presented. I ensured my choice of language was correct, notation correct, figure labels etc... were all correct, which they are to the best of my knowledge. In terms of clarity, I think that I adequately defined everything necessary that whoever reads this will understand the logical structure of the project. References were clearly stated were I thought necessary, and the report was mostly well structured. A change I would consider is small reordering of the final chapter - I do not think what I did is wrong in terms of the organisation of analysis, but more I could have maybe avoided a jump in the differing excitations.